SPECTRAL SHIFT OPERATED SMAHTR TO IMPROVE CYCLE LENGTH AND DISCHARGE BURNUP SIMULTANEOUSLY

A Dissertation
Presented to
The Academic Faculty

by

Vedant Kiritkumar Mehta

In Partial Fulfillment
of the Requirements for the Degree
Master of Science in
Nuclear Engineering

Georgia Institute of Technology
December 2018

SPECTRAL SHIFT OPERATED SMAHTR TO IMPROVE CYCLE LENGTH AND DISCHARGE BURNUP SIMULTANEOUSLY

Approved by:

Dr. Dan Kotlyar, Advisor
Nuclear and Radiological Engineering
Georgia Institute of Technology

Dr. Bojan Petrovic
Nuclear and Radiological Engineering
Georgia Institute of Technology

Dr. Chaitanya Deo
Nuclear and Radiological Engineering
Georgia Institute of Technology

Date Approved: November 30, 2018

To the ones focused on securing energy resources for the future while also minimizing its

negative impact on climate change

ACKNOWLEDGEMENTS

TABLE OF CONTENTS

LIST OF TABLES

LIST OF FIGURES

LIST OF SYMBOLS AND ABBREVIATIONS

AHTR	Advanced High Temperature Reactor
BOL	Beginning of Life
BWR	Boiling Water Reactor
CHM	Carbon-to-Heavy Metal ratio
CTC	Carbonate Thermochemical Cycle
DOT	Department of Transportation
DRACS	Direct Reactor Auxiliary Cooling System
EOL	End of Life
FC	Fabrication Cost
FCC	Fuel Cycle Cost
FHR	Fluoride High-temperature Reactor
LRM	Linear Reactivity Model
LWR	Light Water Reactor
ME	Moderating Elements
MSR	Molten Salt Reactor
ORNL	Oakridge National Lab
PB-FHR	Pebble-Bed Fluoride High-temperature Reactor
PF	Packing Fraction
PHX	Primary Heat Exchanger
PWR	Pressurized Water Reactor
SmAHTR	Small modular Advanced High Temperature Reactor
SS	Spectral Shift
T/H	Thermal Hydraulic
TRISO	TRistructural-ISOtropic
UxC	Ux consulting company

SUMMARY

Fluoride High Temperature Reactors (FHRs) are envisioned to be next generation reactors due to their inherent safety design characteristics and high efficiency from their use of salt-based coolants. FHRs use TRistructural-Isotropic (TRISO) fuel for its benefits of encapturing fission gases and fission products in its layers. One of the main disadvantages of using TRISO fuel is that its fabrication costs are a lot higher (in range of $5,000-$30,000 per kg Uranium) compared to current pellet-based fuel ($300 per kg Uranium). In this study, we propose and develop a spectral shift method to operate this type of reactors. This spectral shift method is based on varying neutron energy spectrum. As a result, both cycle length and discharge burnup are improved simultaneously while eliminating the need of burnable poison.

CHAPTER 1.   INTRODUCTION

Fluoride-salt-cooled High Temperature Reactors or FHRs are a new generation of reactors which will eliminate many drawbacks of current fleet of reactors such as Light Water Reactors (LWRs) and Boiling Water Reactors (BWRs). FHRs are thermal spectrum reactors which operate at near atmospheric pressure and higher coolant temperatures (600℃ to ∼1000 ℃). These reactors use tri-isotropic (TRISO) fuel, graphite as moderator and molten-fluoride-salts (e.g. FLiBe, FLiNaK) as coolant [7]. Thermal properties such as heat capacity of these salts are very advantageous due to its capability of removing decay heat passively. Another big advantage comes from the use of multi-layered spherical TRISO fuel. This fuel consists of a central fuel kernel encapsulating several external layers of graphite-based media which captures fission products and fission gases, thus making it highly accident tolerant against the release of fission products in coolant.

In spite of all the safety enhancements attained by using FHRs, the fuel fabrication costs of TRISO, having such advanced geometry, contributes to one of the most significant drawbacks. The fuel fabrication cost (FC) for TRISO are estimated between $5000 and $30,000 per kgU with $10,000 per kgU being its nominal cost. In comparison, commercial UO_2 based fuel costs $300 per kgU in fabrication costs. To be economically competitive with other energy sources in market, reduction in Fuel Cycle Costs (FCC) is required.

Due to such high fabrication costs, even a fractional gain in discharge burnup will result in significant benefits in FCC. This is the main motivation of this study. Our primary objective is to provide an operational scheme for FHRs which will result in higher fuel utilization and thus lower costs. We propose a scheme denoted as the Spectral Shift (SS)

which relies on continues neutron energy spectrum variation within the reactor core aimed to provide higher cycle length and thus higher discharge burnup. Spectral Shift is achieved by reducing the amount of Moderating Elements (ME), *i.e.* graphite in our case, at the Beginning-of-Life (BOL). This induces a harder spectrum in reactor core leading to fission neutrons being captured in ^{238}U yielding ^{239}Pu. Graphite is then continuously inserted till the End-of-Life (EOL) to maintain criticality and burn the extra bred ^{239}Pu. As a cumulative result, higher in-core residence time is obtained.

For our study, we chose Oak Ridge National Lab (ORNL) developed concept of Small-modular Advanced High Temperature Reactor (SmAHTR) [9]. SmAHTR is a compact, truck transportable 125 MW$_{th}$ thermal spectrum reactor designed to deliver safe, affordable, and reliable high temperature process heat and electricity. CHAPTER 2 provides detailed background on this reactor core, materials, and geometry. In CHAPTER 3, methodology for performing Neutronic, Thermal-Hydraulic (T/H), and Spectral Shift analysis is provided. Detailed results along with discussions for a real-world practical implementation of Spectral Shift scheme are provided in CHAPTER 4. Finally, we summarize our results and conclude our study in CHAPTER 5 providing potential scope to extend this study. The methodology, results and discussion provided in this thesis were also published in conferences and journal papers ([25], [26], [27], [28]).

CHAPTER 2.   BACKGROUND

In this chapter, the background for SmAHTR is provided. The first section covers the history and the motivation for developing SmAHTR. In the second section, several core design selections are provided for SmAHTR. Furthermore, details regarding the selection of materials, and geometry for SmAHTR are included in this section. In the third section, a newer design aiming to use SmAHTR to produce efficient hydrogen is defined and chosen as our reference design. In the fourth and final section, details regarding the development of the proposed spectral shift method is summarized.

2.1   An Overview of SmAHTR

Fluoride-salt-cooled high-temperature reactors (FHRs) are a new generation of reactors known for their use of liquid-fluoride-salt-coolants, graphite moderators, and accident tolerant tri-isotropic (TRISO) fuel. Fluoride salts have higher boiling temperature (>1200 ℃), graphite is both a moderator and reflector, and TRISO fuel can capture fission products and fission gases in its layers thus preventing its release in coolant. FHRs, unlike Molten Salt Reactors (MSRs), do not use both fuel and coolant as its working fluid. FHRs employ near-atmospheric pressure and high coolant temperature output (600℃ to ~800 ℃). Higher coolant output is associated with higher thermodynamic efficiency and hence better energy conversion. These characteristics make FHRs commercially very attractive compared to the current fleet of reactors like LWRs.

Small-modular Advanced High Temperature Reactor (SmAHTR) is a 125 MW$_{thermal}$ FHR reactor concept and a smaller scaled design of a 3400 MW-thermal Advanced High

Temperature Reactor (AHTR), designed at Oakridge National Lab (ORNL) in 2010 [9]. A diagram of SmAHTR primary system is provided in Figure 1. Many of the core concepts and configuration for SmAHTR relies on the design characteristics developed for AHTR [6]. For example, fuel, coolant, moderator, vessel wall material etc. were all adopted from AHTR design space. If material challenges are met allowing even temperature outputs of > 700℃, SmAHTR could further be used to produce hydrogen through electrolysis, petrochemical refining, steam-methane reformation and more. Therefore, a reliable SmAHTR system would revolutionize other high temperature applications as well.
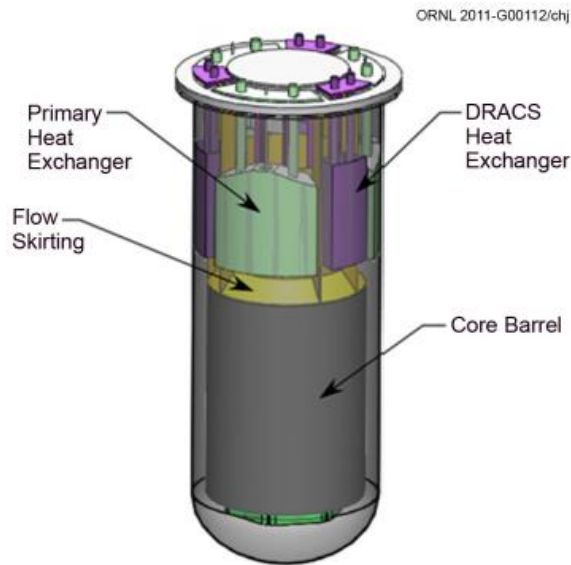
Figure 1 – SmAHTR design by ORNL [9]

SmAHTR is designed with primary intent to provide safe, affordable, and reliable high temperature heat and electricity. SmAHTR consists of a "two-out-of-three system" scheme for its heat removal system. In other words, only two out of three Direct Reactor Auxiliary Cooling System (DRACS) loops are required to remove decay heat during reactor operation and shutdown. Furthermore, the heat is passively removed by natural convection, which makes this reactor safe in an accident scenario. It contains of all its

primary components embedded inside the reactor vessel allowing it to be transportable and assembled to remote sites. ORNL envisioned standard tractor-trailer transportation system is shown in Figure 2.
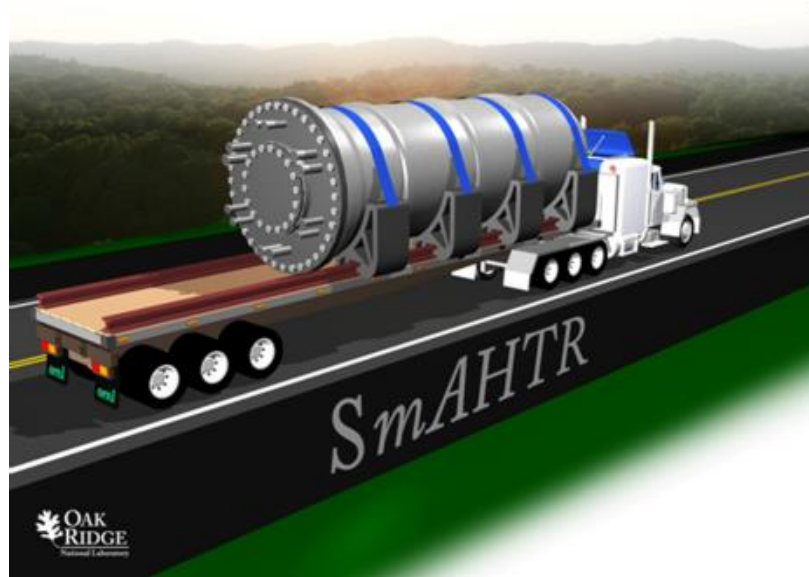
Figure 2 – Truck transportable SmAHTR system [9]

The SmAHTR initial concept, with the goal of delivering safe, reliable, and affordable high-temperature process heat and electricity, was conceptualized based on certain functional criteria. These design goals were developed after careful considerations of lessons learned from original AHTR work and also acknowledging the challenges that need to be encountered before deploying an unconventional system like SmAHTR. These requirements are outlined below [9].

1. Reactor power level of 125 MW$_{thermal}$

2. Maximum operational fuel temperature of 1250 ℃

3. Reactor core outlet temperature of 700 ℃

4. Passive decay-heat removal capacity of 1% of full power

5. Reactor vessel and internals transportable via standard 53 feet commercial tractor-trailer system

6. Thermal-to-electric power conversion efficiency of greater than 40%

7. System architecture and technology suite that can be adapted to higher temperatures

These requirements were formed to emphasize the 2010 state of SmAHTR. Requirement 1 is dictated by the dimensions constraints and the thermal limits. Requirement 2 prevents the release of fission products from TRISO fuel to coolant. Requirement 3 ensures that Hastelloy-N could be applicable for current reactor vessel. Requirement 4 enforces the requirement of transient decay-heat removal systems during an event of accident or shutdown. Requirement 5 is required by Department of Transportation (DOT) regulations for a maximum allowed truck-transportable system on road. Requirement 6 allows high electricity conversion from high temperature coolant output and the use of Brayton power conversion system. Requirement 7 allows reactor innovation and modification for higher temperature applications (800-1000 ℃) if the future state of technology and research allows. For example, if materials sustaining higher temperatures were to be developed, then Requirement 3 would be modified.

Under this specified functional criteria, the design values for SmAHTR were established. The basic core and operational parameters are outlined in Table 2-1. The reactor power was rated at 125 MW$_{thermal}$ with 9.4 MWt/m^3 volumetric power density. FLiBe and FLiNaK were chosen to be the primary and secondary coolant salt respectively. In the original design, fuel enrichment of 19.75 $wt.$ % was chosen with 50% packing fraction (PF), but in upcoming sections, this will be varied. Graphite was used as both

primary moderator and core reflector. Further details about the core materials and geometry are provided in next section.

Table 2-1 – Original SmAHTR design space [9]

Variable	Value
Reactor Power (MWt)	125
Core volumetric power density, $MW(t)/m^3$	9.4
Primary coolant salt	FLiBe, 99.995% ^{7}Li purity
Fuel type	TRISO
TRISO packing fraction, vol. %	50
Fuel enrichment, wt. %	19.75
Core uranium loading at BOL, kg	1600-2020
Core life, years	4.19
Fuel configuration	Annular pins
Fuel pin diameters (inside, outside), cm	2.2, 6.5
Fuel surface coating thickness, cm	0.3
Moderator material	Graphite
Moderator configuration	Pins and blocks
Moderator pin diameter, cm	6.16
Number of total fuel assemblies/blocks	19
Number of core assembly rings	3
Number of fuel pins/assembly	15
Number of graphite pins/assembly	4
Core height, m	4
Core effective diameter, m	~2.2
Reflector configuration and material	Radial, graphite blocks
Reflector diameter, effective inside, outside, m	~2.2, 3
Vessel height, m	9
Vessel diameter, m	3.5

Table 2-1 (continued)

Vessel wall thickness, cm	2.5
Vessel weight (empty, no lid), kg	22,516
Vessel and skirt material	Hastelloy-N
Secondary coolant salt	FLiNaK
Core cooling mode	Forced convection
Core flow direction	Upward
IHX/downcomer flow direction	Downward
Number of main coolant pumps	3
Number of PHXs	3
Number of DRACS	3
PHX/DRACS annulus, height, m	2
PHX/DRACS annulus, diameter-inner, m	2.365
PHX/DRACS annulus, diameter-outer, m	3.5

2.2 Core Materials and Geometry for SmAHTR

2.2.1 Materials

2.2.1.1 Tri-Isotropic Fuel

As mentioned previously, FHRs use an accident-tolerant Tri-Isotropic (TRISO) structured fuel. As seen in Figure 3, TRISO consists of a multi-layered structure with fuel kernel in the center. TRISO fuel were originally used for gas-cooled reactors but was later adopted for FHR concepts including AHTR and SmAHTR due to their resistance against release of radionuclides at very high temperatures [12]. The fuel kernel of TRISO consists uranium in $UC_{0.5}O_{1.5}$ form. Uranium kernel could have varying enrichment in this fuel

structure (19.75% enriched for 2010 SmAHTR). The UCO fuel kernel is covered by four

additional isotropic graphite shells – porous buffer, inner pyrocarbon, silicon carbide, and

outer pyrocarbon. All combined, these outer layers trap fission products and fission gases

against accidental release. The density and thickness of TRISO were adopted from the

NEUP report published on the study of liquid salt cooled reactors [29] and is provided in

Table 2-2. To prevent the accidental release of radionuclides from TRISO, maximum fuel

temperature cannot exceed 1250℃. TRISO particles are mixed in a graphite bed with a

certain volumetric packing fraction (50% was originally adopted for 2010 SmAHTR). This

mixed configuration with TRISO particles and graphite bed is referred to as fuel. The

geometry of this fuel could be configured based on reactor type *i.e.*, pebbles, plates, pins

etc.

Table 2-2 – TRISO particle properties

Region	Parameter	Dimension (μm)	Density (g/cm^3)
Fuel kernel	diameter	427	10.9
Porous graphite buffer	thickness	100	1
Inner Pyro-Carbon	thickness	35	1.9
Silicon Carbide	thickness	35	3.2
Outer Pyro-Carbon	thickness	40	1.87
TRISO particle	diameter	847	
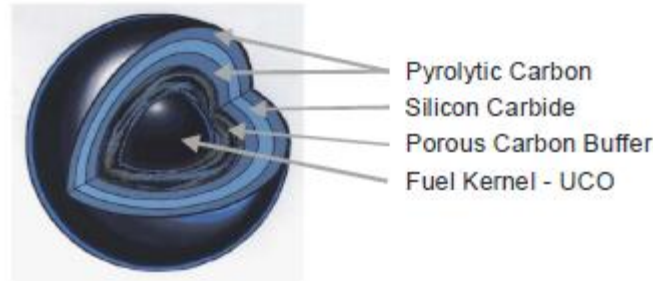
Figure 3 – TRISO coated fuel [12]

Regardless of the many advantages provided by TRISO fuel, its biggest drawback comes from its fabrication costs. Due to its complex geometry and small size (~847 $microns$), the fabrication costs of TRISO fuel are estimated to be between \$5,000 to \$30,000 per kgU with \$10,000 per kgU being the nominal costs [35]. For comparison, current commercial UO_2 fuel pellets fabrication costs are \$300 per kgU.

2.2.1.2   <u>FLiBe Coolant</u>

There are several criteria that a material needs to satisfy for its selection as a primary coolant for a reactor design. For SmAHTR, FLiBe ($2LiF\text{-}BeF_2$) was chosen as primary coolant because it satisfied the following requirements [9].

1. Melting point below 550 ℃ with 100 ℃ refreezing margin.

2. Vapor pressure below 1 atm in all temperature regime.

3. Boiling point above any accident temperatures.

4. Low viscosity with high heat capacity at operation temperatures.

5. Low neutron-absorption cross section.

6. Elements are chemically compatible with core and primary loop materials.

FLiBe with 2:1 ratio of ^{7}LiF to BeF$_2$ was chosen for SmAHTR. The 2:1 ratio minimizes high viscosity of pure beryllium fluoride at SmAHTR operating temperature [9]. By choosing this ratio, the melting temperature of pure ^{7}Lithium Fluoride is reduced from 845°C to 459°C. FLiBe has similar heat capacity to water at 4680 $kJ/(m^3 K)$ which features a very low vapor-pressure. FLiBe can also maintain liquid state without a need a pressurization up to 1400°C [10]. One major limitation of FLiBe is that Lithium needs to be enriched at 99.995% ^{7}Li to minimize the parasitic absorption of neutrons by ^{6}Li.

2.2.1.3   Graphite moderator

For SmAHTR, graphite serves two purposes – (i) a neutron moderator, and (ii) a neutron reflector. Regardless of the core geometry, *i.e.* pin type, plank type, etc., graphite structures are integrated between the fuel elements for many FHR designs. Graphite is attractive as both moderator and reflector due to following characteristics. Graphite:

1. Has low absorption cross-section with high moderating ratio.

2. Is relatively cheap.

3. Has high scattering cross-section.

4. Has a very high melting point of ~4500°C [33].

2.2.2   *SmAHTR core geometry*

Three primary core designs were chosen as candidates for SmAHTR – solid cylindrical fuel (Figure 4), annular cylindrical fuel (Figure 5), and hexagonal plank fuel (Figure 6). Neutronic and thermal-hydraulic studies were performed for all three designs by ORNL [9]. In each of these fuel designs TRISO fuel relied on 19.75% enriched uranium

in form $UC_{0.5}O_{1.5}$. TRISO particles were assumed to be loaded with 50% packing fraction

for first two designs, prismatic blocks and annular cylinders, while 40% packing fraction

for hexagonal plank design.

2.2.2.1   Stacked prismatic blocks

For the first cylindrical type stacked design, both graphite and fuel are in form of

pins assembled inside a single fuel block as shown in Figure 4a. Each fuel assembly (Figure

4) consists of hexagonal graphite that encompasses 72 fuel pins and 19 graphite pins. Each

of these blocks is 0.8 $meter$ in height. Five blocks are vertically stacked to give a total

height of 4 m. Nineteen fuel blocks with 45 cm pitch are hexagonally packed to complete

one stack of five vertical stack. Coolant flows through each fuel assembly and through the

outer coolant channels. This type of design is also referred to as stacked prismatic blocks

with stringer fuel bundles.

The depletion studies for this core configuration resulted in cycle length of 3.52

$years$ for 1556.4 kg of 19.75% [235]U enrichment. The reactivity coefficients were

calculated using fuel, coolant, and graphite for 1100℃-1500℃ interval. The overall

reactivity coefficient was -2.70 pcm/K [9].

a. Fuel block   *b. Core cross section*
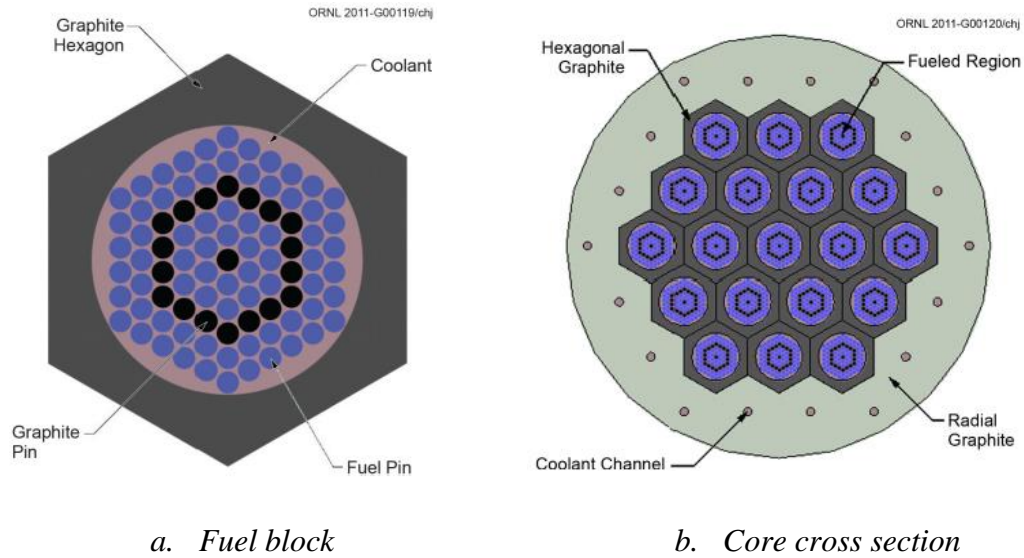
Figure 4 – Cylindrical fuel-type geometry [9]

Even though this core provided sufficient neutronics and thermal performance, there were two major issues with this fuel form – (i) fabricating long cylindrical fuel form is very challenging, and (ii) the centerline fuel temperature is relatively high due to the cylindrical pins configuration. To mitigate these two issues, annular fuel form was investigated.

2.2.2.2   Annular cylindrical bundles

For the annular cylindrical bundles concept, fuel is configured into 5 cm high "beads" (Figure 5a) strung along a vertical carbon rod. These beads have 3 mm thick graphite sleeves for protection against erosion. Fifteen vertical fuel stacks are required one fuel assembly (Figure 5b). Nineteen assemblies are required for a single core as in previous geometry. This geometry consists of 1806.7 kg of uranium. Coolant is allowed to flow from both inside the fuel assembly and through the outer holes as in first design.

From the neutronics studies, cycle length for this configuration was found to be 4.19 $years$. The overall reactivity coefficients for same temperature interval were -3.12 pcm/K for this geometry.

ORNL 2011-G00122/chj

Graphite

ORNL 2011-G00124/chj

Coolant

Fuel Annulus

Tie Rod

Graphite Pin

a. *Single annular fuel bead*   b. *Fuel bundle assembly*
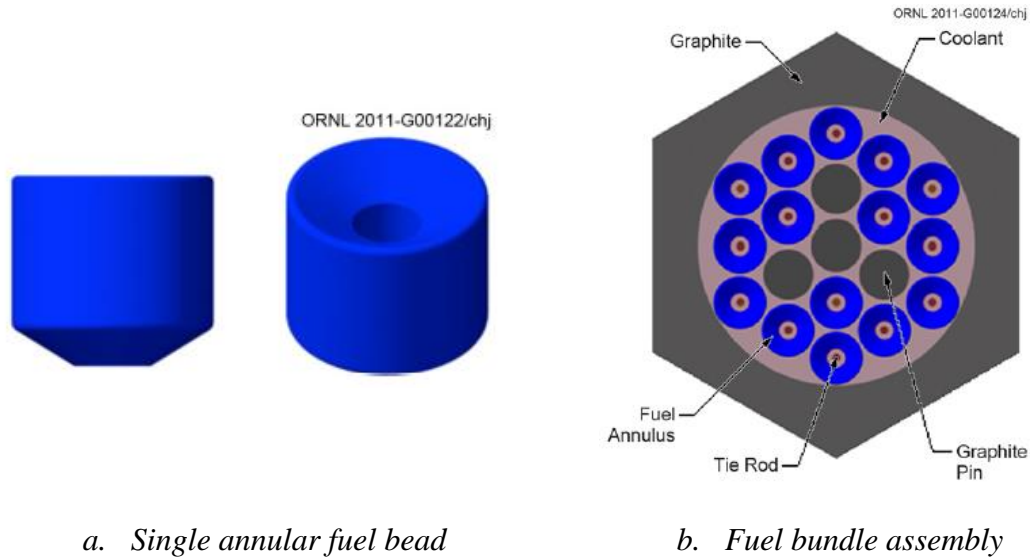
Figure 5 – Annular cylindrical fuel [9]

Previous studies [9] showed that annular fuel design decreased the maximum fuel temperature, however, this fuel form would result in component vibrations caused by coolant flow which would limit fuel lifetime. As a result, third, plank mechanical fuel structure was investigated.

2.2.2.3   Hexagonal fuel plank

In the original hexagonal plank or plate-type design, one fuel assembly consisted of three symmetric regions, each consisting of five or six fuel plates. These plates have non-fueled ridges that provided mechanical stability by preventing flow induced vibrations. In the center of this assembly, a "Y-shape" separated five fuel plates (Figure

6a). This Y-shape acted as a composite support which allows significant ease to loading and refueling of this fuel. For a six plate per one-third region design, every other plate consists of fuel (*i.e.* 3 per one-third assembly) and remaining plates consist of graphite. Coolant is allowed to flow in-between these plates and through outer coolant channels. Each fuel plate consists of $2\ mm$ graphite edges to prevent erosion from coolant flow. Total of nineteen fuel assemblies are needed for a single core. The central fuel region in the core consists of two out of three regions with six fuel/graphite plates each while the third region is used for control rod insertion (Figure 6b).

Unlike previous two designs, this design consisted of 40% TRISO packing fraction with a total mass of 2015.4 kg uranium in the core. Even with such high fuel content compared to previous two designs, cycle length for plank-type design was only 3.08 $years$.

a. *Single assembly of 5 fuel-planks*   b. *Core cross section*
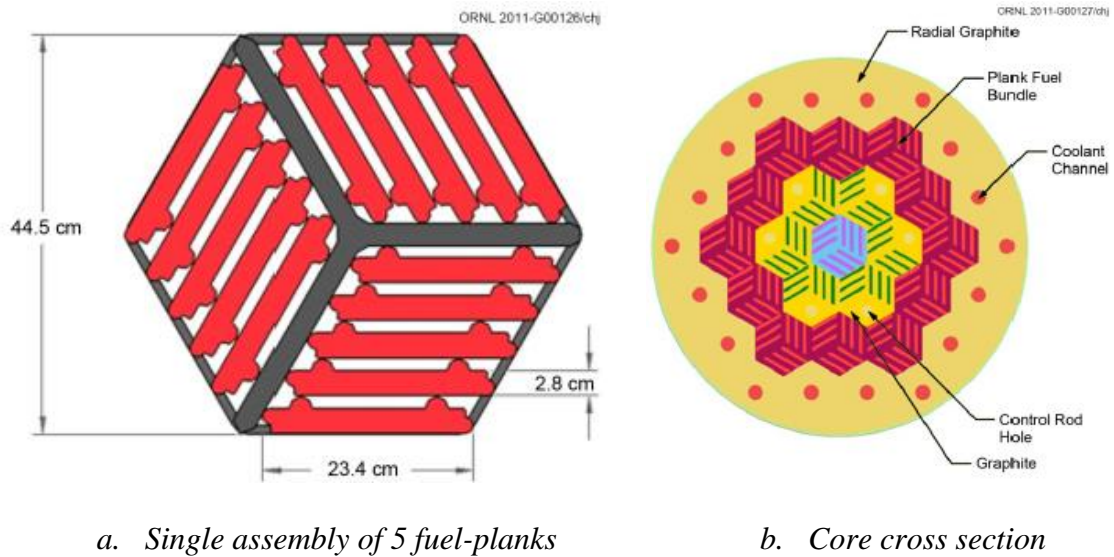
Figure 6 – Hexagonal fuel plank [9]

This fuel form was more mechanically stable due to its mounting compared to both cylindrical and annual fuel-type. However, neutronic and thermal-hydraulic results for

plank fuel configuration were not as attractive as the other two fuel forms and thus ORNL [9] called for a requirement of additional investigation for this fuel form. Thermal-Hydraulic (T/H) results from original study [9] are provided in Table 2-3. Accordingly, due to its mechanical integrity and easier refueling scheme as a cartridge, plank-type fuel is adopted and further investigated in this study.

Table 2-3 – T/H results from original SmAHTR investigation [3]

Fuel configuration	Diameter or thickness (cm)	Total number of pins or plates in the core		Coolant temperature (°C)			Max fuel temp. (°C)	Flow (kg/s)			Vortex valve diodicity
		Fuel	Graphite	Lower plenum	Max	Top plenum		Pump	Core	Bypass	
Cylindrical pins/stringers	2.8	72 × 19	19 × 19	650	700	695	1,178	350	1018	32	400
				650	715	700	1,182	350	969	81	50
Annular pins	2.2–6.5	**15 × 19**	**4 × 19**	650	737	700	1,143	350	905	145	50
				650	**703**	**687**	**1,027**	**510**	**1325**	**205**	**50**
Plates	2.6	18 × 19	0	650	703	700	975	350	1003	47	50
	2.8	9 × 17	9 × 17	650	706	700	1,240	350	949	101	50
	2.8	12 × 17	12 × 17	650	719	700	1,023	350	757	293	50
	2.8	12 × 17	12 × 17	653	700	686	1,002	530	1096	494	50
	2.8	12 × 17	9 × 17	651	700	694	1,061	410	1100	130	50

[a]Cylindrical and annular pins are located inside hexagonal graphite blocks. Plate fuel does not have the hexagonal graphite blocks. The total number of assemblies in the core is 19. For the four last cases (plate fuel), 6 control rods occupy 2 full assemblies; thus, the total number of fueled assemblies is only 17. The *Reference Design fuel* is in bold: fourth line—Annular Pins with high pump/core flow and reduced coolant temperatures.

2.3 Repurposed SmAHTR design: SmAHTR-CTC

In 2014, a redesigned reactor concept called SmAHTR-CTC was presented [11]. The Carbonate Thermochemical Cycle or CTC would allow SmAHTR to enable efficient hydrogen production. The CTC concept was adopted from the original SmAHTR work [9] and from 2012 efforts towards AHTR design [39]. It was then applied to advance SmAHTR core design. CTC concept made several substantial modifications to the original 2010 core design. These modifications are listed below.

1. Due to reactor's small size, hexagonal fuel plank design was chosen as default design since this design could mechanically be handled as a cartridge.

2. Fuel enrichment was changed from 19.75% to 8 wt % ^{235}U/U.

3. Instead of a plate fully loaded with fuel, plate with two fuel stripes was integrated (Figure 7).

4. The assembly-to-assembly pitch was changed from 45 cm to CTC optimal case of 60 cm (as shown in Figure 8).

The new fuel plate design was deducted as having the optimum Carbon-to-Heavy Metal ratio to achieve the longest burnup (*i.e.*, fuel utilization). CHM is the ratio of the number of carbon atoms to the number of fuel atoms in the fuel assembly. CHM could be controlled by changing the size of the central matrix in Figure 7. As an example, if central matrix thickness is zero, it would resemble a fully loaded plate with fuel or CHM of 100. SmAHTR-CTC paper found CHM of 200 to be optimum for their analysis. The overall graphite to heavy metal ratios in the core are ~270, 560, and 1200 that correspond to fuel assembly CHM of 100, 200, and 400 respectively.
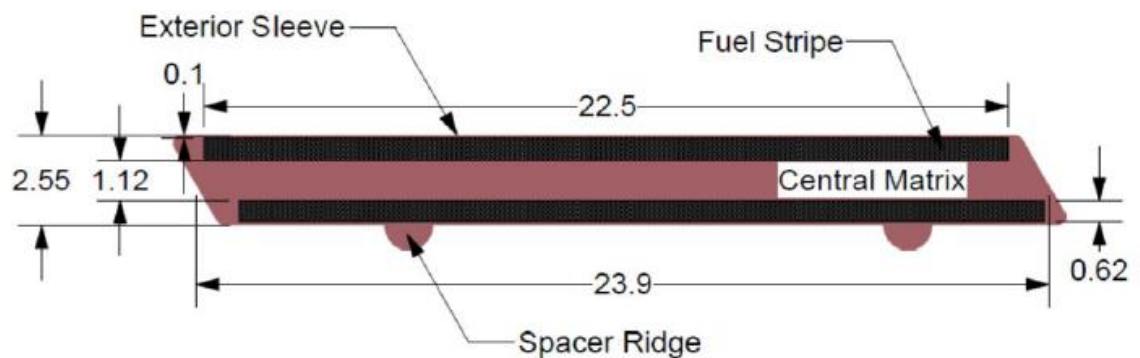
Figure 7 – 2012 AHTR fuel plate [39]
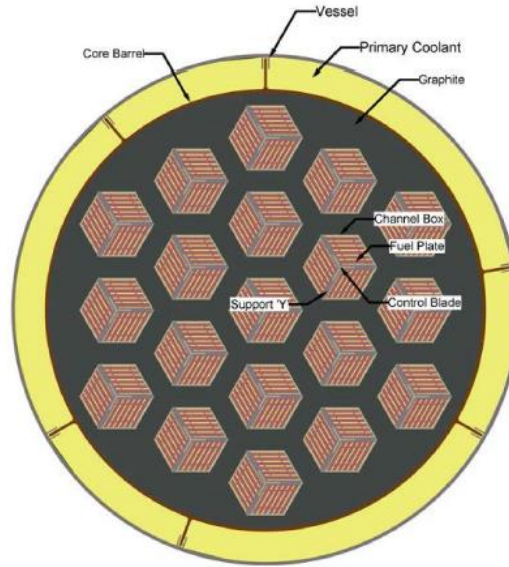
Figure 8 – SmAHTR-CTC core configuration [11]

The spectral shift approach, adopted here, is investigated using the 2010 SmAHTR design with modifications provided by the 2014 CTC design. Next section provides an overview of spectral shift regime.

2.4   Overview of Spectral Shift

Spectral Shift (SS) is a terminology used to describe the change in neutron energy spectrum inside a reactor core. This is done by controlling the reactor materials in such a manner that it allows neutron energy spectrum to shift between BOL and EOL. In past, this concept was applied as a proof-of-concept to model many reactor systems. In practice, however, the spectral shift operational regime is not heavily applied, with the exception of BWR systems, in which the mass flow rate is adjusted towards the end-of-cycle to create a softer spectrum and earn extra days of operation. Spectral shift control was originally proposed in 1961 by Mars and Gans [23]. Their study focused on changing the ratio of $D_2O:H_2O$ in a pressurized water reactor (PWR) to increase fuel utilization. At BOL, the

core started with high concentration of heavy water. Heavy water is then continuously diluted with increasing light water until the EOL. It was suggested that the spectral shift method offered both technical and economic advantages compared to reactor control with burnable poison. Since then, several other designs incorporating spectral shift were investigated. In 1980, Ronen and Galperin [32] showed that spectral shift control by mechanically varying V_m/V_f ratio of light water could theoretically achieve twice as increase in burnup compared to spectral shift through shift in $D_2O:H_2O$ ratio in LWRs. Yokomizo et al. proposed the use of "spectral shift rod", a water rod with varying recirculation rate, to manage reactivity [41]. It eliminated the need for control rods throughout the burn and increased uranium savings.

In recent years, spectral shift efforts have started focusing on new generation of reactor designs. A 2018 study applied spectral shift to Transatomic Power MSR to increase fuel utilization [1]. In 2017, a spectral shift proof of concept using SmAHTR annular fuel pin design was presented [14]. This design incorporated the change in V_m/V_f ratio by changing graphite density as a preliminary analysis. Results of this design showed fuel utilization improvements by more than 40%. However, this study focused on original 2010 SmAHTR design with 19.75 wt % [235]U enrichment and 50% TRISO packing fraction.

Research in this thesis adapts work performed by Kotlyar et al [14] by taking modifications proposed by SmAHTR-CTC design. In addition, this study focuses on a more realistic investigation of the spectral shift approach for SmAHTR by including the spatial effects into account. For SmAHTR-CTC, Spectral Shift is applied by changing the volume of moderating elements inside the core and thus changing the V_m/V_f ratio. The

graphite moderator in between the fuel assemblies (Figure 8) is utilized to vary the graphite quantity in the core and thus to operate under the spectral shift regime. At the BOL, large portion of graphite is removed from the system, only fractional graphite is retained to start the reactor critical. This imposes a harder spectrum in the reactor allowing neutrons to escape resonance regions of ^{238}U and breed ^{239}Pu. Increased ^{239}Pu adds to the amount of fissile material available in the reactor. To maintain the reactor critical, the removed portion of graphite is then continuously inserted until the EOL. As a result, the extra ^{239}Pu that was produced earlier is utilized towards the EOL, thus extending both the cycle length and the discharge burnup of the core simultaneously.

CHAPTER 3.   CODES AND METHODOLOGY

In this Chapter, a detailed description of the codes and methods used to perform this study is provided. Section 3.1 describes the Serpent, Monte Carlo based, code and the T/H model used to analyze the thermal performance for both the original and the proposed designs. The core and burnable poison design, and the chosen model to assess the discharge cycle length and burnup are described in Section 3.2. This section also outlines the implementation of the spectral shift paradigm used to perform the calculations for the proposed design.

3.1   Codes and methods

3.1.1   Serpent

For neutronics analysis, Serpent, a continuous-energy Monte Carlo reactor physics burnup calculation code, was utilized [16]. Serpent provides several benefits over other Monte Carlo (MC) codes. MC methods are very accurate and hence used for neutron transport calculations for reactor applications. However, since the Monte Carlo method is based on random sampling, it is computationally intensive. To improve the general MC performance, Serpent uses Woodcock delta-tracking method-based routine, which makes it more computational efficient compared to the conventional methods such as surface-to-surface ray-tracing implemented by most MC codes [18]. Furthermore, SmAHTR, being FHR, incorporates TRISO based fuel, Serpent's has a built-in functionality to generate randomized particle distribution using the SHAKE algorithm, which was used in the current study.

3.1.1.1 Overview of Serpent

A brief description of the Monte-Carlo (MC) method is presented in this chapter. In addition, the main difference between Serpent and standard MC codes is explained.

Monte-Carlo based codes rely on random neutron sampling to track the transport of neutrons. MC codes allow to obtain the continuous space, energy, and angular distribution for even the most complicated geometries. MC tracks a limited number of neutrons in a given system. The position, velocity magnitude and direction are sampled to start the tracking routine of these neutrons in a given medium. The neutrons interact with the material and the outcome depends on the energy-dependent material cross-section probabilities. Each of these neutrons is tracked from the time it was born till it is absorbed or leaked out of the system. The more complicated the geometry and the associated material distribution, the more computational expensive the tracking routine becomes. This is simply the result of using standard ray tracking routine, according to which the sampling distance to the next collision depends on the material and hence cross-sections. However, the neutron can pass multiple material boundaries and thus the traveling distance must be updated according to the material type. In general, the distance to the next collision is sampled from a Cumulative Distribution Function (CDF). The Probability Distribution Function (PDF) of a particle encountering a collision at an arbitrary distance x is given as

$$f(x) = \Sigma_t e^{-x\Sigma_t}. \qquad\qquad (1)$$

The CDF can be obtained by integrating the PDF over distance x.

$$F(x) = \int_0^x \Sigma_t e^{-x'\Sigma_t}\, dx' = 1 - e^{-x\Sigma_t}. \tag{2}$$

Uniformly distributed variable ξ selected on a unit interval which provides a value of corresponding exponentially distributed variable x through the inverse function of the CDF given below

$$F(x) = \xi \Longleftrightarrow x = F^{-1}(\xi). \tag{3}$$

The neutron distance to the next collision site could be sampled by using the inversion method as

$$x = -\frac{1}{\Sigma_t}\ln(1-\xi) = -\frac{1}{\Sigma_t}\ln(\xi) \tag{4}$$

where random number ξ_i is defined by $\xi_0 \in [0,1]$ for a new neutron or the neutron that has underwent a collision with collision/boundary index being i.

One of the biggest drawbacks of neutron transport codes comes from having numerous material regions in a given geometry. Since properties vary from material to material, so does the material cross-sections. Therefore, in most MC codes, neutrons are tracked from one material surface to the other which provides certain neutron interaction with that material. If the collision distance, x, is less than the distance to the next material surface, the particle position in updated based on its initial position, $\bar{p}$, and its direction or line-of-sight $\bar{\Omega}$.

$$\vec{p'} = \vec{p} + x\vec{\Omega} \tag{5}$$

On the other hand, if the collision distance p is greater than the distance to the material boundary, B, then the particle is transported to the boundary, material cross-sections are updated and the residual property ξ_{i+1} is used to specify the remaining collision distance.

$$\xi_{i+1} = e^{\Sigma_t(x_i - B_i)} \tag{6}$$

$$x_{i+1} = -\frac{1}{\Sigma_t}\ln(\xi_{i+1}) \tag{7}$$

This is known as surface-to-surface tracking or ray-tracing algorithm. Calculating the distance to the nearest surface is done by calculating distances to all cell boundaries in a neutron's "line-of-sight" and then obtaining its minimum value. It is easy to observe that when a high energy neutron crosses multiple surfaces, this method becomes very time consuming and computationally expensive.

An alternative to this method is provided by Delta-tracking where surface crossings are eliminated. During a neutron lifetime, several non-absorbing interactions occur where a neutron's incident energy and direction of flight doesn't change. These interactions are called pseudo-scattering reactions or virtual collisions. The main idea of delta tracking method lies behind these virtual collisions. There will be an arbitrary number of virtual collisions that a neutron experiences during its lifetime which would not affect its statistics. Delta-tracking method adds a virtual collision cross-section to materials such that the modified total cross-sections is same in all materials. This virtual cross-section (Σ_0) is defined as

$$\Sigma_0(r, E) = \Sigma_m(E) - \Sigma_t(r, E) \qquad (8)$$

where Σ_t is the total cross-section of material as before, and Σ_m is the maximum of the total cross-section, or the majorant cross-section of all the materials. This allows neutron to sample a real or virtual collision without recording surface crossings. By implementing such a technique, Serpent obtains significant speed-up in reactor physics calculations. The collision distance using the newly defined majorant cross-section is

$$x = -\frac{1}{\Sigma_m} \ln(\xi_0) \qquad (9)$$

A rejection technique counteracts the process of whether or not to accept virtual cross-section. If the virtual cross-section has to be accepted, then a random number, η, needs to meet the criteria $\eta < \frac{\Sigma}{\Sigma_m}$, with $\eta \in [0,1]$. The real cross-section at the virtual collision location is simply

$$\Sigma = \Sigma(\vec{p} + x\vec{\Omega}). \qquad (10)$$

The PDF of Woodcock delta-tracking method is equal to the surface tracking algorithm. However, the derivation will not be covered here. The mechanisms behind Serpent's reactor physics calculations through particle handling in a multi-material media and its implementations of delta-tracking is much more advanced than that presented in this section. However, it is not the scope of this study and it is only provided to serve as a lead-in to Serpent methodology and application.

3.1.1.2 Modeling through Serpent

Serpent allows the user to model a reactor geometry as 2-dimensional infinite, or 3-dimensional with a rated thermal power. This is done by defining cells, surfaces and applying boundary conditions. The materials are then defined for each cell or region. These materials utilize given cross-sections for individual nuclei which Serpent uses to perform Monte-Carlo depletion step. User defines neutron populations for each cycle, and the amount of active and inactive cycles. These cycles and neutron histories play a huge role in the accuracy of the solution. Higher the histories, more accurate the solution. Serpent provides numerous outputs such as plots, nuclide history, neutron flux, criticality in specific regions, and more. Upon defining burnup steps, Serpent outputs multiplication factor as a function of burnup or time in Effective Full Power Days (EFPD) which can be utilized to determine the cycle length for a given reactor configuration. Serpent was used for all neutronics analysis carried out in this study. The main parameters collected from Serpent's outputs included multiplication factor, time-dependent spatial isotopic concentrations, and 3D time-dependent spatial power distributions used by the T/H model to calculate the temperature distribution within the core.

3.1.2 *Thermal-Hydraulic Model*

A Thermal-Hydraulic (T/H) analysis is necessary to investigate whether spectral shift regime would deteriorate the thermal performance of the SmAHTR design. Both hottest channel analysis and full 3D core T/H calculations were performed. For T/H analysis, the THERMO code was utilized [15]. The THERMO module was developed for the coupled MC BGCore code to provide T/H feedback by calculating fuel, gap, cladding and coolant

26

temperatures and densities at predetermined burnup steps. The module is suitable for analyzing a wide range of geometries, such as square or triangular pitch fuel pin lattices and block-type fuel. In the current research, a plate-type geometry was added to the calculation sequence. In addition, a thermo-physical properties database for diverse coolant, fuel and structural materials of current reactors is readily available. For this study, the database was extended to include the properties of silicon carbide (SiC) [36] and FLiBe ([40], [37]).

The methodology relied on calculating the pressure losses in separate T/H channels. Friction, form, acceleration and gravity pressure losses are all accounted in the T/H analysis. Since the pressure drop distribution among parallel coolant channels must be identical, an iterative routine to calculate the mass flow rate distribution is implemented. The iterative approach relies on the Newton-Raphson method to obtain uniform pressure losses in all channels through variation of the flow rate in each channel. The procedure starts with uniform mass flow rate guess and stops when the relative difference between the minimum and maximum pressure loss values is below 0.1%.

3.1.2.1 Radial Conduction Model

A simplified 1-D conduction is assumed in our model *i.e.* no heat conduction in axial direction. Heat is convected axially by the coolant and hence this is a 1.5D model. The temperature distribution in the plank fuel surrounded by the FLiBe coolant with a graphite sleeve in between is solved by the general steady-state 1-D heat conduction equation:

$$\frac{d}{dx}\left[k(T)\frac{dT}{dx}\right] + q''' = 0 \tag{11}$$

The inner wall fuel temperature (*i.e.,* T_f) at the fuel surface (*i.e.*, $x = a$) is obtained using:

$$T_f = \left(\frac{1}{h} + \frac{\delta_s}{k_s}\right) \cdot q'' + T_\infty \tag{12}$$

where, h is the heat transfer coefficient, k_s is the conductivity of the graphite sleeve and δ_s is the thickness of the sleeve. The power density, q''', in each layer is known directly from Serpent. The bulk FLiBe coolant temperature is sequentially updated for each axial layer.

Finally, the maximum fuel temperature of the TRISO particles at the center of the slab ($x = 0$) is calculated by applying:

$$\int_{T_f}^{T_m} k_{fuel}(T)dT = \frac{q'''}{2}a^2 \tag{13}$$

In order to solve and evaluate the fuel temperature distribution within the fuel (between $x = 0$ and $x = a$), it is divided into 10 equal-volume 1-D layers and Equation **13** is solved iteratively until a converged fuel temperature distribution is achieved.

3.1.2.2   T/H Properties

This section presents the properties used in this study. The thermal conductivity of the fuel meat, *i.e.*, TRISO particles embedded within a graphite matrix, was estimated according to a model described by Lewis [20]. The thermal conductivity of uranium

dioxide was obtained from the mentioned study and is represented by the following relation:

$$k_{UO_2}\left[\frac{W}{m\,°K}\right] = \begin{cases} 10.41 - 9.44 \times \dfrac{T}{10^3} + 2.52 \times \left(\dfrac{T}{10^3}\right)^2 & T < 1800 \\ 1.73 & T \geq 1800 \end{cases} \quad \textbf{(14)}$$

The thermal conductivities for the graphite and silicon carbide were fitted according to the data points presented by Matsuo [24] and Snead et al. [36] and the correlation are presented in Equation **15** and Equation **16**, respectively.

$$k_{gr}\left[\frac{W}{m\,°K}\right] = 131.2 - 0.08432T + 1.96 \times 10^{-5}T^2 \quad \textbf{(15)}$$

$$k_{SiC}\left[\frac{W}{m\,°K}\right] = 114{,}885.7 \times T^{-1.02233} \quad \textbf{(16)}$$

It is possible [20] to derive a mathematical relation for the mean or effective conductivity of the composite material in terms of the volume fraction of the coated particles and the conductivity of the matrix materials. Kerner [13] derived such an expression, in which spherical particles were coated by another material and dispersed in a matrix as shown in Equation **17**.

$$k_{fuel}\left[\frac{W}{m\,°K}\right] = \frac{k_{gr}V_{gr} + k_{UO_2}V_{UO_2}\gamma_{UO_2} + k_{SiC}V_{SiC}\gamma_{SiC}}{V_{gr} + V_{UO_2}\gamma_{UO_2} + V_{SiC}\gamma_{SiC}} \quad \textbf{(17)}$$

where the weighting factors γ_{UO_2} and γ_{SiC} are evaluated using the expressions presented in Equation **18** and Equation **19**.

$$\gamma_{UO_2}$$

$$= \frac{9k_{gr}k_{SiC}}{(k_{UO_2} + 2k_{SiC})(k_{SiC} + 2k_{gr}) + 2\left(\frac{V_{UO_2}}{V_{UO_2} + V_{SiC}}\right)(k_{gr} - k_{SiC})(k_{SiC} - k_{UO_2})} \tag{18}$$

$$\gamma_{SiC}$$

$$= \frac{3k_{gr}(k_{UO_2} + 2k_{SiC})}{(k_{UO_2} + 2k_{SiC})(k_{SiC} + 2k_{gr}) + 2\left(\frac{V_{UO_2}}{V_{UO_2} + V_{SiC}}\right)(k_{gr} - k_{SiC})(k_{SiC} - k_{UO_2})} \tag{19}$$

where V_{UO_2}, V_{SiC} and V_{gr} are the volume fraction of the uranium dioxide, silicon carbide and graphite respectively and $V_{UO_2} + V_{SiC} + V_{gr} = 1$.

3.2 Core design

The SmAHTR-CTC design (Figure 9) was chosen as our base case. Using the parameters and materials from original 2010 SmAHTR design, a 2D core was created using Serpent. This geometry consists of nineteen hexagonal fuel assemblies spaced with pitch of 60 cm. The core consists of graphite moderator, in dark grey, in-between the fuel assemblies. The FLiBe coolant (yellow) flows downwards in-between the vessel wall and outer reflector and then convects heat upwards through the fuel assemblies.

a. Radial view   *b. Axial view*
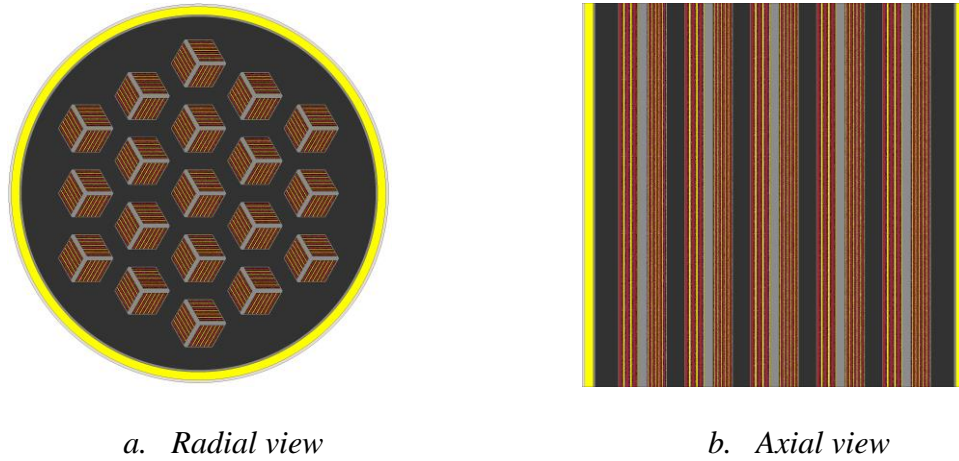
Figure 9 – Serpent built SmAHTR reference design

A symmetric three region six fuel plate detailed cross-section of a hexagonal fuel assembly is provided in Figure 10. The detailed geometric dimensions for this assembly are provided in Table 3-1. This assembly is based on SmAHTR-CTC reference design and thus has CHM of 200. The CHM will be perturbed in this study for spectral shift sensitivity analysis. The Y-shape (in gray), also made of graphite, separates all three fuel regions and also allows the assembly to be mechanically handled as a cartridge. The fuel matrix is shown in purple color, embedded central carbon matrix in maroon color, and coolant in between the fuel plates is denoted by yellow color. The TRISO particles (black dots) are randomly scattered in the graphite bed with 40% packing fraction. There are some particles that are cut-off with the carbon matrix and sleeve due to their randomized distribution which would relate to slight discrepancy in calculating packing fraction. However, this issue has a negligible impact (i.e., several pcm) on the cycle length and thus is not investigated in details in this thesis. The 1 mm carbon sleeve between fuel and coolant protects the fuel from erosion due to coolant flow.
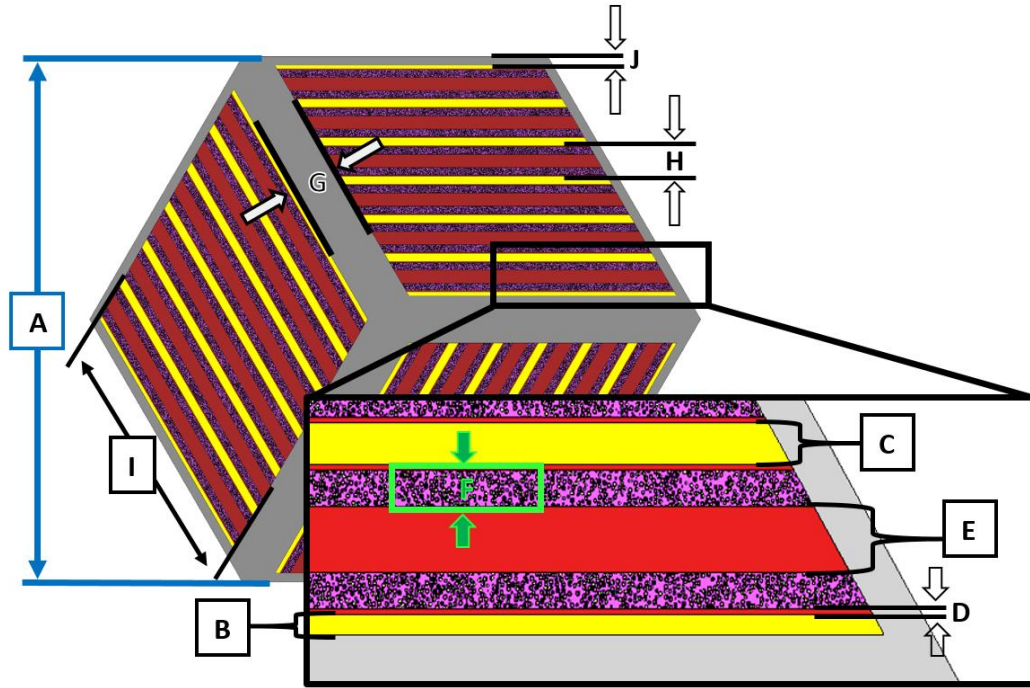
Figure 10 – Detailed cross section of single fuel assembly

Table 3-1 – Detailed fuel assembly dimensions for Figure 10

Region	Description	Size (cm)
A	Fuel assembly flat to flat	45
B	Outer coolant channel width	0.35
C	Inner coolant channel width	0.7
D	Graphite sleeve thickness	0.1
E	Central carbon matrix	1.12[†]
F	Fuel meat thickness	0.62[†]
G	Y-shape breadth	4
H	Single fuel plate width	2.55
I	Fuel plate length	22.5
J	Fuel assembly wall	1.17

[†] Based on SmAHTR-CTC design [11]

3.2.1   Burnable Poison consideration

In previous analysis for SmAHTR (Original [9] and CTC [11]), burnable poison was not considered to suppress the excess reactivity for the original design. However, it was mentioned in the CTC paper that the maximum excess reactivity should not exceed 6% $\Delta k/k$. This is 4% $\Delta k/k$ less than the original AHTR design. The lower maximum excess reactivity originates from the blade's control worth limit. In contrast to the original design, the excess reactivity for the spectral shift approach can solely be controlled by the moderating elements due to the very low reactivity swing; thus eliminating the need of burnable poison. To the best of our knowledge, the use of fixed burnable absorbers for the original SmAHTR design was not studied extensively and was only mentioned in the pre-conceptual design [9]. The authors suggested to manage the excess reactivity swing by mixing Boron carbide (B_4C) in the graphite matrix in conjunction with gadolinium or erbium as coated particles embedded in the same matrix. Additional studies performed for the AHTR design [39] suggested that Eu_2O_3 particles are also a good burnable poison candidate. Therefore, in this study, Eu_2O_3 and B_4C grains were embedded in the carbonaceous matrix at the center of the fuel plate, as shown in Figure 11.
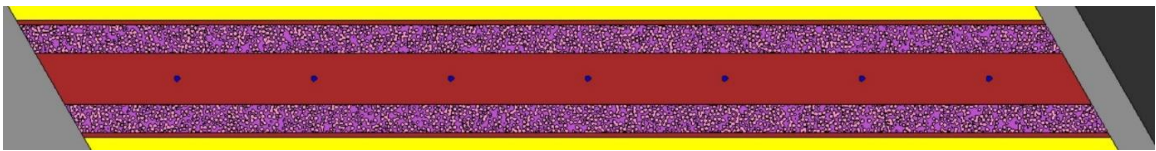

Figure 11 – Burnable poison particles embedded in the central graphite matrix

The main goal of this study was to investigate and include the cycle length penalty by the reactivity swing caused due to the use of burnable poison in the original design.

3.2.2   Multibatch Scheme

For the CTC design [11], a multibatch regime was investigated using the Non-Linear Reactivity Model (NLRM) [4]. More specifically, the discharge time and burnup were predicted for the original CTC design bearing burnable poison and operated under a multi-batch scheme using the NLRM. However, due to the complexity of spectral shift approach, a similar model cannot be applied to estimate spectral shift gain for multi-reloading scheme. Therefore, multibatch scheme was investigated using explicit modelling under the spectral shift control. Two additional refuelling strategies were considered *i.e.* three- and six-batches refuelling strategies, presented in Figure 12. The burnup-level is denoted by 'nx' where, for example, $n = 2$ represents twice-burnt fuel. For each case, an equilibrium cycle was achieved by simulating the full core in conjunction with the spectral shift regime. The compositions for each batch at the end of cycle were set to be the compositions for the next iteration and this iterative procedure was repeated until a convergence was achieved. For the 3-batch case, 6 fresh (0x), 6 once-burnt (1x), 6 twice-burnt (2x), and 1 thrice-burnt (3x) fuel assemblies were used. In the 6-batch case, all the fuel batches relied on three assemblies with the exception of a single fuel assembly for the sixth-burnt (6x) batch. It must be pointed out that these refuelling strategies are based on non-equal batch sizes.

a. Three-batch system   *b. Six-batch system*
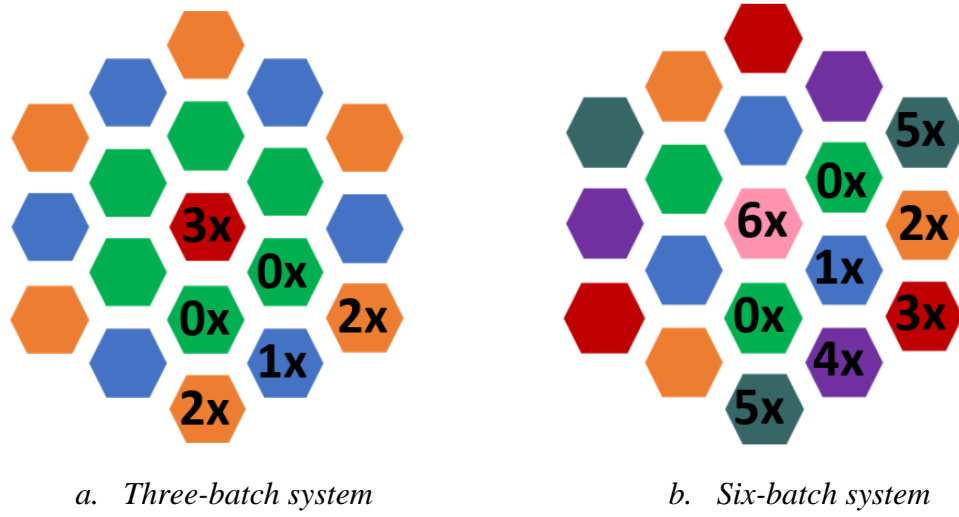
Figure 12 – Multibatch loading pattern

Since the amount of fissile material decreases in the inventory with increasing number of batches, it is expected that the effect of spectral shift or the gain in fuel utilization due to spectral shift will also decrease as per increasing number of batches.

3.3   Spectral Shift

SmAHTR spectral shift relies on the change in V_m/V_f ratio during the core cycle, accordingly, the graphite volume within the SmAHTR core needs to be modified. For this study, several approaches are investigated to apply this spectral shift method.

3.3.1   *Spectral Shift mimicking with varying Graphite density*

For the preliminary sensitivity analysis, variation in graphite density of SmAHTR-CTC design was investigated to mimic spectral shift paradigm. The spectral shift method was applied by changing the density of outer fuel assembly graphite (dark gray in Figure 9a). At the BOL, the graphite density was reduced to minimal requirement just enough to start the reactor. Then as the cycle continues, the density of this graphite is gradually

increased until it reaches 100%. An external algorithm using MATLAB was developed to control the core reactivity. The structure of this algorithm is shown in Figure 13. The routine starts with an initial graphite density of zero. Using this density, Serpent is run to obtain effective criticality. If the criticality is above 1, then a burnup step of certain days is added. If the criticality is below 1, then a fraction of graphite density is added to system. Once a burnup step or fractional density is added, Serpent is rerun to obtain a new criticality. This cycle is repeated until the fractional density of graphite reaches 100% or in other words, until the actual density of graphite is reached.
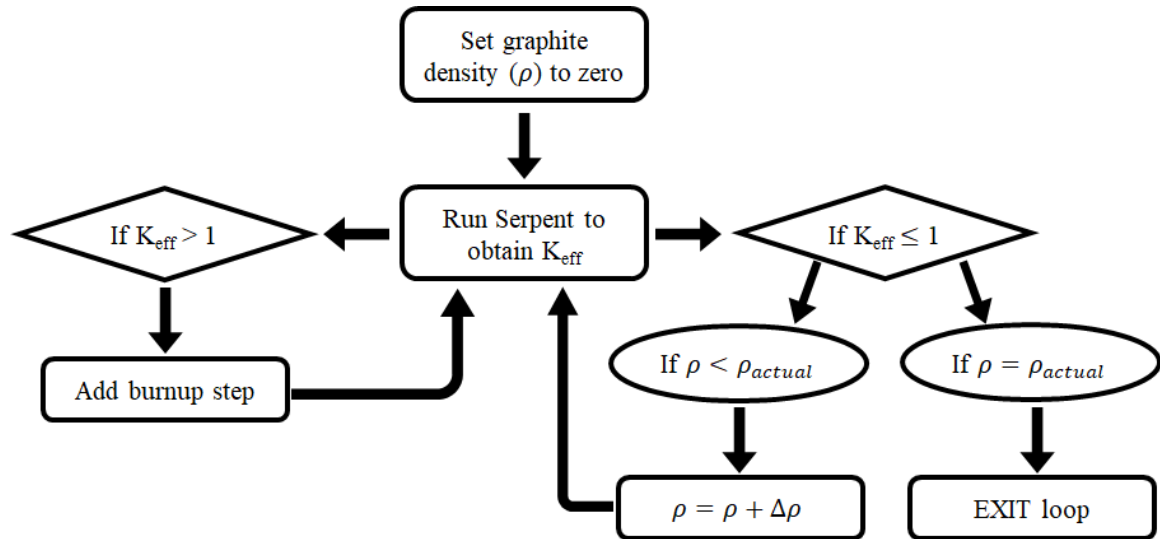
Figure 13 – MATLAB coupled Serpent spectral shift algorithm

The goal of this analysis is to understand the sensitivity of different parameters on fuel utilization. The summary of parameters analyzed in this part are listed in Table 3-2. This study will provide optimal parameters for spectral shift which will be utilized in the next section.

Table 3-2 – Parameters for sensitivity analysis

Parameters	Sensitivity cases
Fuel enrichment	5%, 8%, 19.75%
Assembly-to-assembly pitch (in cm)	45, 50, 55, 60, 65
TRISO packing fraction	30%, 40%, 50%
Carbon-to-Heavy Metal ratio (CHM)	100, 150, 200, 250, 280, 300, 400

Fuel enrichment is the enrichment of the uranium in UCO kernel inside the TRISO fuel. The sensitivity of the distance between adjacent hexagonal assemblies or the assembly-to-assembly pitch were investigated to understand their effect on spectral shift (Figure 14). Pitch of 45 cm refers to assemblies in contact with each other. The percentage of TRISO particles in the graphite bed or the TRISO packing fraction (PF) was optimized as well. Finally, the Carbon-to-Heavy Metal ratio or the CHM was varied by adjusting the thickness of central carbon matrix as shown in Figure 15. Note that CHM of 100 refers to the plate filled without central carbon matrix, while CHM of 400 refers to very thin fuel stripes in each plate.
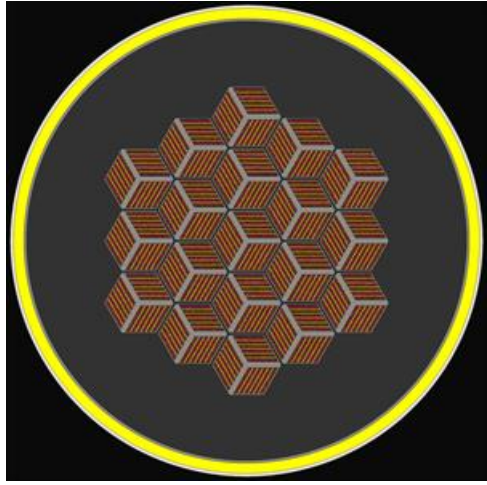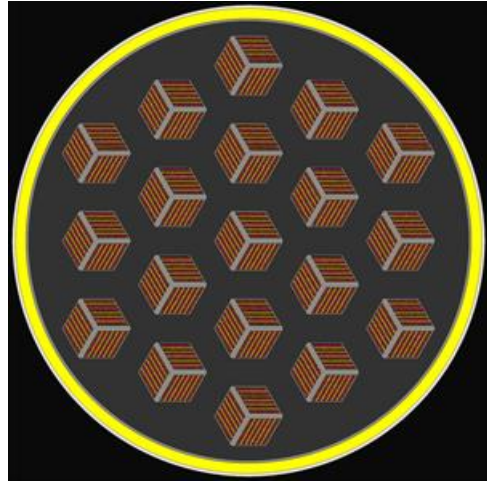
a. Pitch = 45 cm   *b. Pitch = 65 cm*

Figure 14 – Variation of lattice pitch
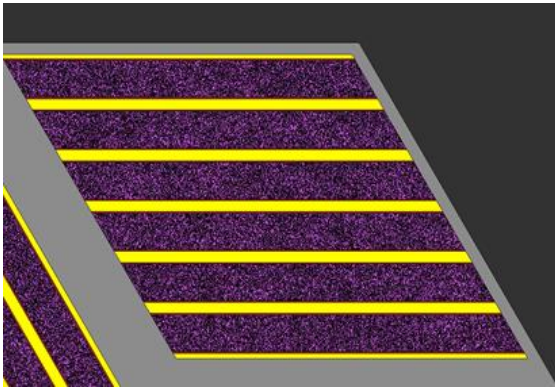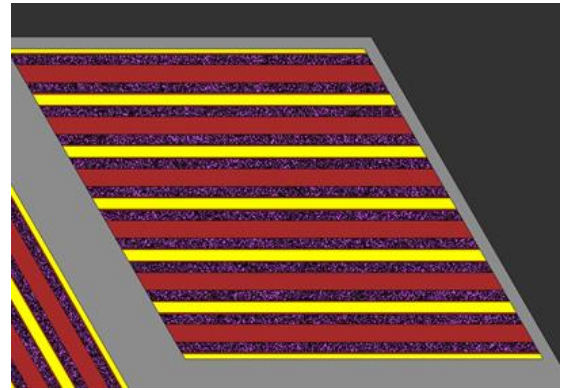
a. CHM = 100   *b. CHM = 200*
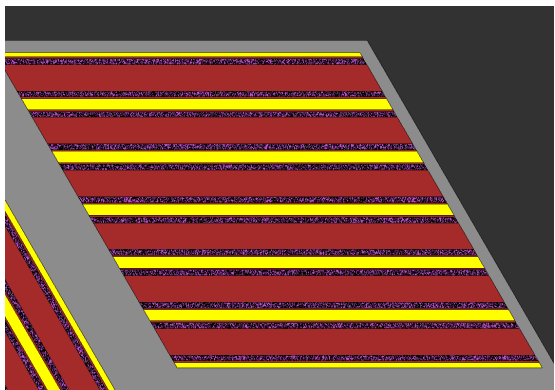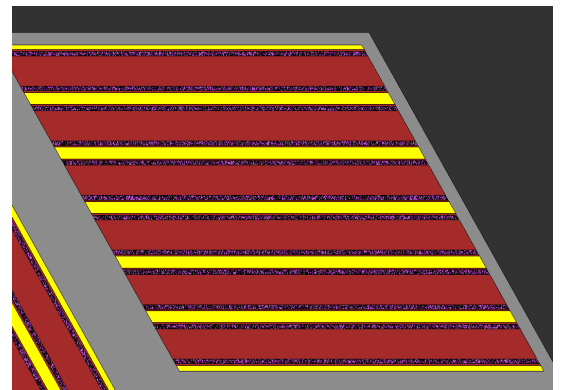
c. CHM = 300   *d. CHM = 400*

Figure 15 – Variation of CHM through change in central matrix thickness

3.3.2 *Spectral Shift with movable graphite blocks*

The methodology described in previous section was used to identify near-to-optimum design space for which detailed analyses were performed to identify most favorable design. In this stage, the spectral shift analysis was extended to test the viability of physical graphite insertion. To do this, the graphite structures in between each assembly were divided into multiple graphite elements. Around each fuel ring (3 in total), 20 equal volume segments were defined in the computational model (Figure 18). The spatial graphite structures were inserted sequentially around each fuel region while maintaining criticality. The latter was achieved by implementing an external criticality search routine that was coupled to Serpent (Figure 16). This routine is very similar to the one used in previous stage with an exception that the graphite density addition is replaced by graphite structure insertion. To maintain criticality in this stage, each graphite structure is inserted one-by-one in the core.
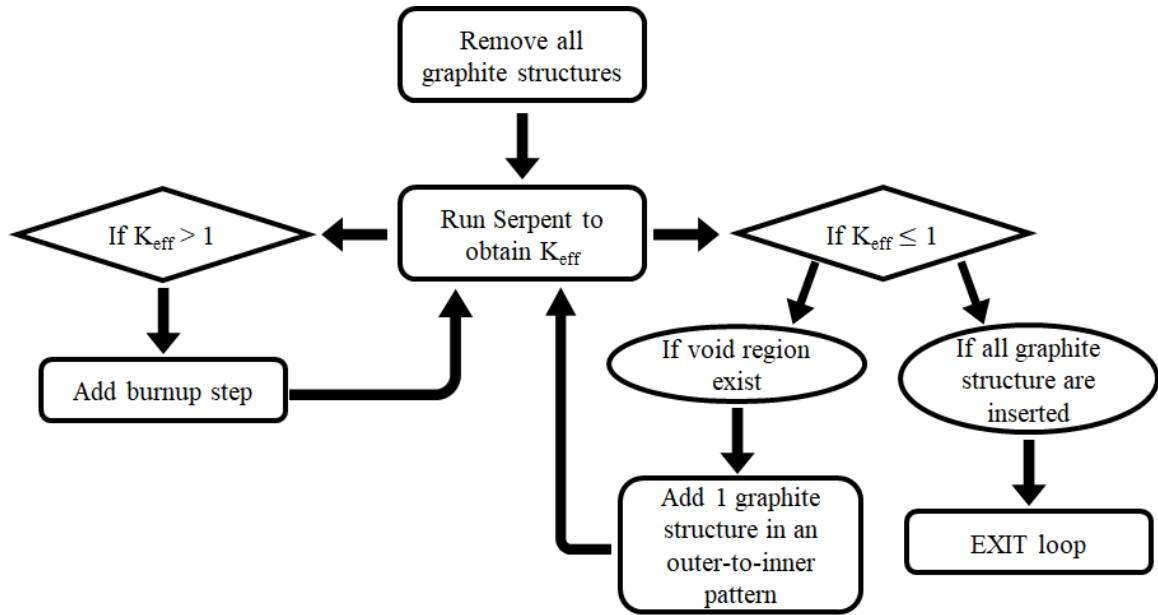
Figure 16 – Spectral shift routine for graphite elements

The practical routine relied on dividing each fuel assembly into the center region, which contained the fuel planks, and twenty peripheral equal volume hexagons, as shown in Figure 18. This division was fixed for all the examined cases (e.g., different assembly pitches) by varying the layers' individual thicknesses. At BOL, these peripheral regions were voided (with no coolant), but were sequentially replaced by graphite material to maintain criticality. The applied spatial reactivity control is still not considered to represent the final practical design, but takes into consideration the spatial effects during such operation regime and hence is more realistic than adjusting the graphite density. The core presented in Figure 17 consists of 3 concentric radial rings with 12, 6 and 1 fuel assemblies going from the outermost to the innermost ring. The graphite insertion pattern was chosen to be from the outer region to the inner region as shown in Figure 17b. The motivation to use the outer-to-inner graphite insertion relies on reducing the neutron leakage that leads to a less efficient fuel utilization.
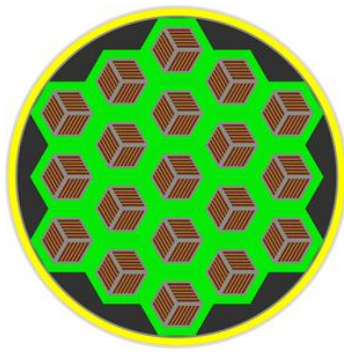
a. *"Hard" spectrum. Graphite structures removed.*
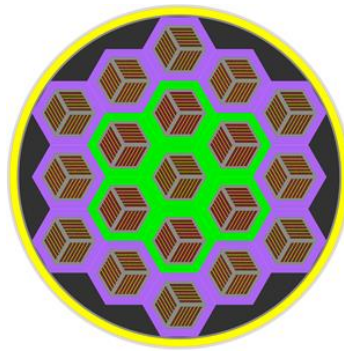
b. *Intermediate spectrum. Graphite structures partially inserted.*
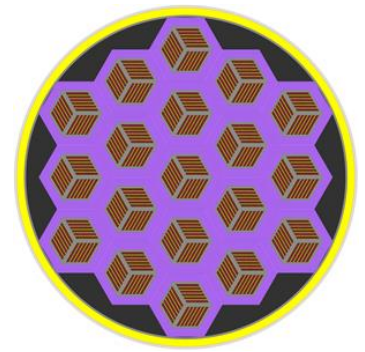
c. *"Soft" spectrum. Graphite structures fully inserted.*

(voided regions in green, inserted graphite in purple)

Figure 17 – Graphite block concentration from BOL to EOL
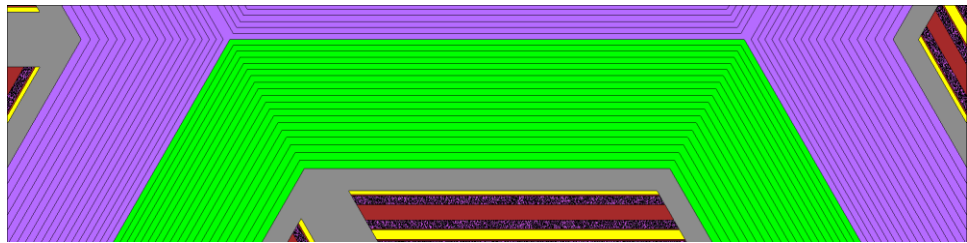
Figure 18 – Spatial discretization of equal volume graphite elements

CHAPTER 4.   RESULTS AND DISCUSSION

This chapter contains the results obtained in numerous studies performed for SmAHTR spectral shift paradigm. These studies are outlined below.

- Neutronic studies including the sensitivity studies for original and spectral shift design are presented in Section 4.1.

- Thermal Hydraulic analysis for the original and proposed (*i.e.* spectral shift) design are proposed in Section 4.2.

- Economic models and fuel cycle costs for both original and proposed design are provided in Section 4.3.

- Finally, results for potentially a practical spectral shift scheme realization based on a molten moderator is proposed in Section 4.4.

Neutronic studies cover sensitivity for both the original and the proposed designs. These sensitivity studies rely on mimicking the spectral shift through graphite density change. Using such a methodology a fast screen of multiple cases can be performed to identify a near-to-optimum (or more converged) design space. This stage is followed by accounting for the spatial effects via the variation of graphite spatially in the core. The results from the graphite-based structures provided a more realistic spectral shift gain and hence were compared with the original SmAHTR-CTC design. Multiple multi-reloading schemes for SmAHTR were investigated and compared against the original design. The reactivity coefficients that serve as indicators to safety metrics were also calculated for both the original and the proposed designs operated under one- or multi-batch schemes.

Thermal performance was investigated next to calculate the thermal limits for both designs. This study focused on the maximum centerline fuel temperature as the limiting factor by explicitly analyzing a 3D full core.

Finally, the fuel cycle costs were calculated for both designs based on the cycle length and discharge burnup calculations obtained from Section 4.1. This analysis included the costs associated with multibatch system and burnable poison.

In the last section, we provide a potential realizable approach to implement the spectral shift system- future work. It must be pointed out that even though this work focused on the SmAHTR or similar FHRs, the designs, approaches, and results undertaken for this core could be applied to other FHR designs. More details on design selection are provided in this section and in the last chapter.

4.1   Neutronic Results

4.1.1   Original Design

SmAHTR-CTC [11] was chosen as a reference design for this study. The original SmAHTR-CTC studies included optimizing the fuel utilization performance. However, the mentioned studies did not account for burnable poison to control excess reactivity. Therefore, in this study, the original design is further investigated, and the analyses are extended by accounting for burnable poison. From here on, SmAHTR-CTC will be referred to as the 'original design'.

4.1.1.1 Optimal SmAHTR-CTC Design

The reference design showed that the cycle length of ~2 $years$ is possible with enrichment of 8%. This research used an optimum assembly-to-assembly pitch of 60 cm and CHM of 200. CTC study showed that increasing pitch from original 2010 design of 45 cm to higher pitch provided significantly higher fuel utilization. It was also suggested that pitch higher than 60 cm increased the core neutron leakage. The trade-off between the decreased resonance capture (*i.e.* lower absorption) of ^{238}U and increased neutron leakage is shown in Figure 19. Increasing the lattice pitch results in reduced system absorption rate and increased leakage rate. Therefore, an optimum pitch size will result in maximum fuel utilization. The reduced absorption rate is due to the more heterogeneous design, which leads to more efficient moderation and finally results in reduced resonance capture by ^{238}U in the epi-thermal energy range, as shown in Figure 20.
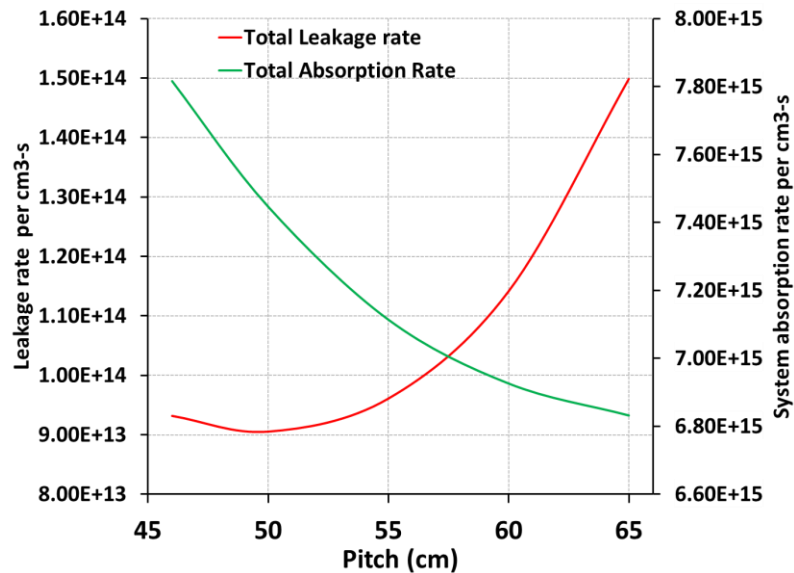
Figure 19 – Leakage and Absorption rate as a function of pitch
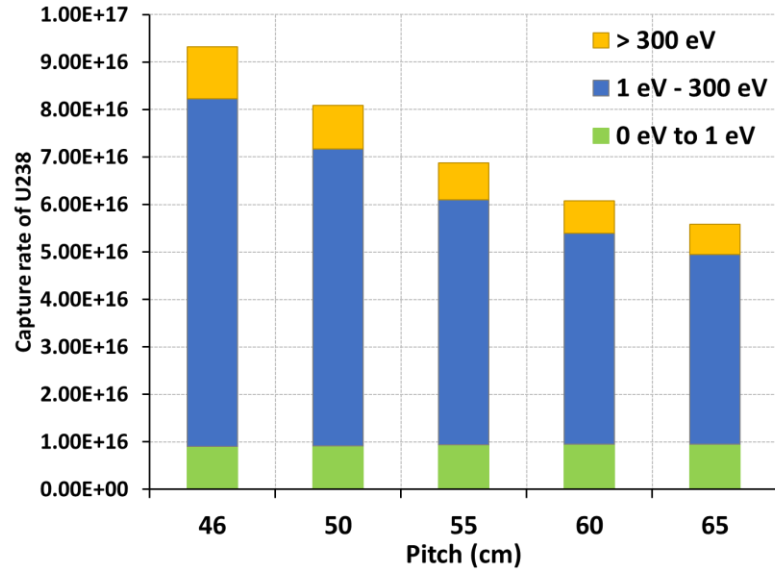
Figure 20- Capture rate of ^{238}U with varying pitch size

The criticality curve for optimum SmAHTR-CTC cycle is shown in Figure 21. This design has a BOL effective criticality of ~1.36. The green region, defined by SmAHTR-CTC paper to be $6\%\ \Delta k/k$, shows allowed operational region for SmAHTR. The cycle length for this design is 744 $days$ with a discharge burnup of 49.5 MWd/kgU.
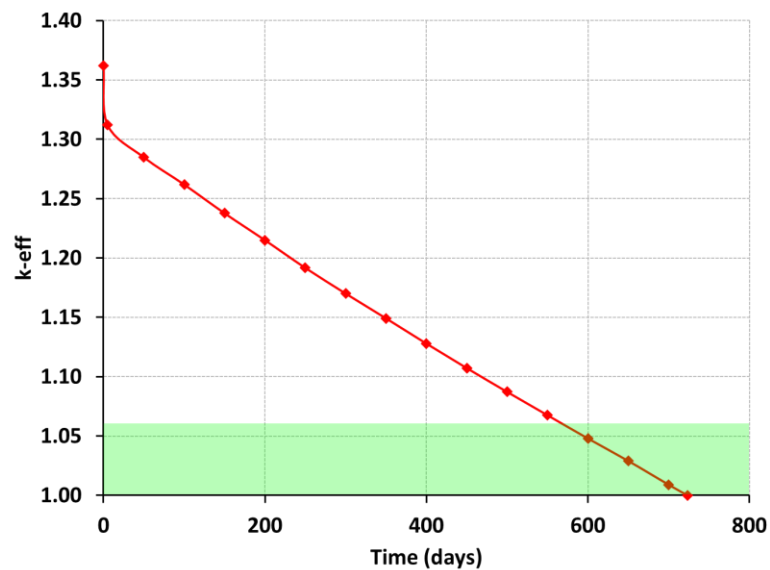
Figure 21 – Original SmAHTR-CTC design

4.1.1.2 SmAHTR-CTC with Burnable Poison

To properly account for cycle length penalty, burnable poison investigation is necessary. Adopting the AHTR burnable poison approach [39], burnable poison powdered spheres were implemented in SmAHTR. To manage the excess reactivity swing, Boron carbide (B_4C) is mixed in the graphite matrix in conjunction with gadolinium or erbium as coated particles embedded in the same matrix. It was also suggested that Eu_2O_3 particles are also a good burnable poison candidate. Therefore, in this study, Eu_2O_3 and B_4C grains were embedded in the carbonaceous matrix at the center of the fuel plate as shown in Figure 11. This is the BISO or Bistructural Isotropic particle mechanism. A rigorous burnable poison analysis was performed for LSCR applications where BISO and QUADRISO (Quadruple Isotropic) particles were implemented as burnable poisons [8]. Selecting the type of poison, particle type, and location would influence the reactivity and cycle length penalty. QUADRISO particles are same as TRISO particle but with an extra layer of burnable poison. Due to higher fabrication costs of TRISO-like particles, BISO particle mechanism is adopted here. As a first attempt of the study, the burnable poison was defined as either Eu_2O_3 or B_4C particles. It was decided to change the number of particles embedded within the matrix from 0, *i.e.* no burnable poison, to 8. In addition, the radius of the particles was varied up to 0.1 cm. Figure 22 presents just a sample of criticality curves when the burnable poison is chosen to be B_4C. In this case, a 0.07 cm radii of each spherical particle were used. This figure shows that increasing the number of particles does reduce the reactivity swing but using more than 6 particles creates a sub-critical configuration. The criticality curves for the Eu_2O_3 burnable poison are shown in Figure 23. It seems that

using more than 8 particles may reduce the maximum reactivity requirements below 6% $\Delta k/k$, however the cycle length penalty is too large.
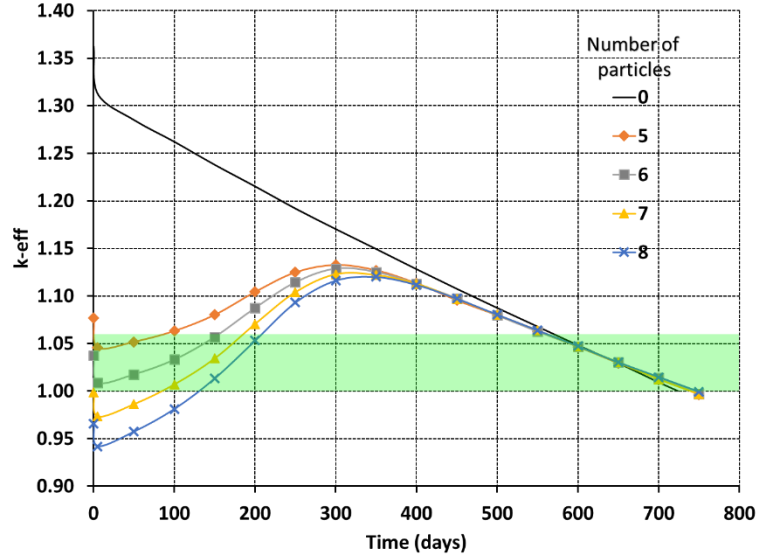
Figure 22 – Criticality curves for varying number of B_4C particles
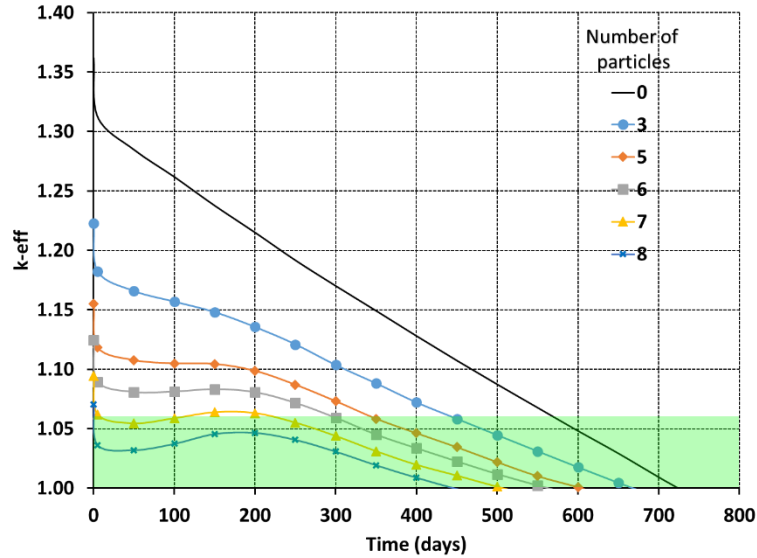
Figure 23 – Criticality curves for varying number of Eu_2O_3 particles

The analyses were also extended to include the combination of these two burnable poisons *i.e.* Eu_2O_3 and B_4C. This stage consisted of varying the radius of the particles (up to $0.1\ cm$) and the total number of particles (up to 10 particles), and finally the fraction of

Eu_2O_3 (relative to B_4C). The main objective was to identify the optimum design set, which maximizes the cycle length (*i.e.* lowest cycle penalty) and yet satisfies the $6\% \, \Delta k/k$ constraint. In order to reduce the computational requirements, Serpent was executed separately for the Eu_2O_3 and B_4C cases to produce the criticality curves for various combinations of particle numbers and dimensions. Then, an external routine, using MATLAB, was implemented to identify the optimum Eu_2O_3 weight fraction ($i.e. \, wt_{Eu_2O_3}$), according to the following relation:

$$k_{eff}(t) = wt_{Eu_2O_3} \cdot k_{eff,Eu_2O_3}(t) + (1 - wt_{Eu_2O_3}) \cdot k_{eff,B_4C}(t) \qquad \textbf{(20)}$$

The results obtained using the linear approximation assumption (Equation **20**) may deviate from the real behavior, however, the purpose of this exercise was only to estimate the possible cycle length penalty. The most favorable case is presented in Figure 24, in which a maximum cycle length of $702 \, days$ is achieved ($42 \, days$ penalty). The optimum weight fraction of Eu_2O_3 was found to be 66% (consisting of $N = 2$ particles with $R = 0.07 \, cm$ radius), where the remaining fraction of B_4C consisted of $N = 10$ particles with $R = 0.1 \, cm$ radius.
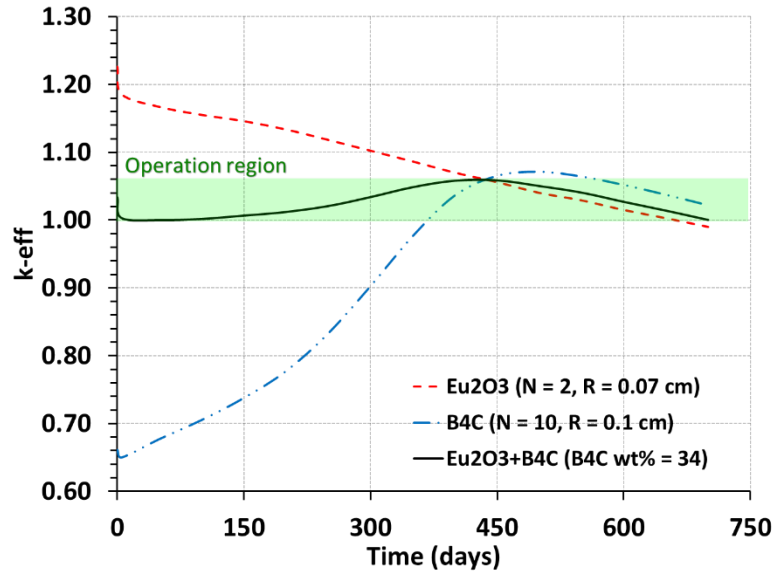
Figure 24 – Weighted k$_{eff}$ as a function of time using Eu_2O_3 and B_4C

The final comparison is presented Figure 25. Original case with (w/ Burnable Poison) and without burnable poison (w/o Burnable Poison) are provided. Minimum cycle length penalty of $42\ days$ was achieved with the most optimized burnable poison mixture.
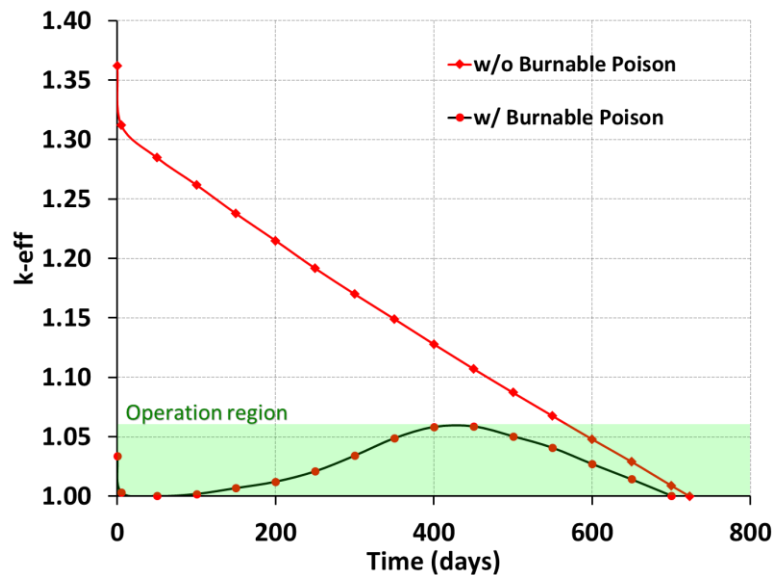
Figure 25- Original case with and without burnable poison

Finally, the mentioned above approach was used to study the cycle penalty (in days) for different allowable reactivity swings (previously defined as 6% $\Delta k/k$). The results are

49

reported in Figure 26. Negative cycle length penalty indicates that longer irradiation periods can be achieved due to the harder spectrum induced by using strong thermal absorbers.
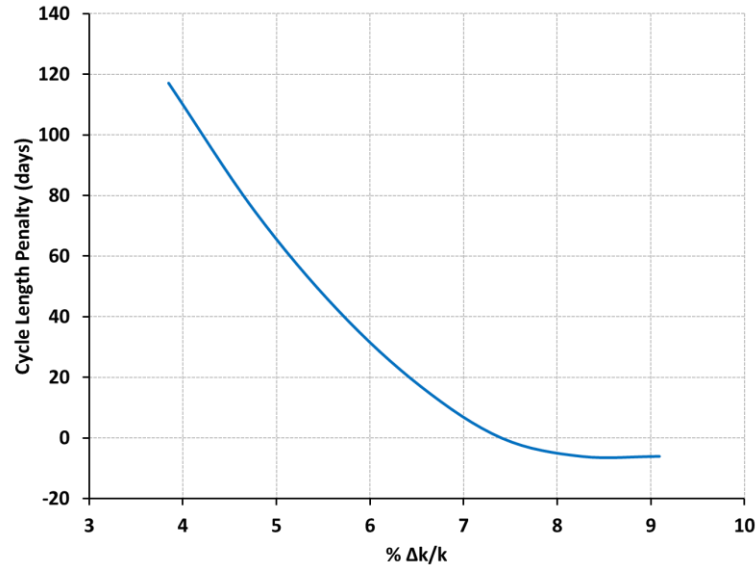
Figure 26 - Cycle length penalty for various $\%\Delta k/k$

4.1.2 Proposed Design

For the preliminary sensitivity analysis, the goal was to obtain near to optimum design by performing coarse sensitivity studies. To do so, i) Carbon-to-Heavy Metal ratio (CHM) and assembly-to-assembly pitch were varied from 100-400 and 46-65 cm respectively. Same analysis was repeated for original design for initial comparison. The initial results were obtained by mimicking the spectral shift control by density change. Such an approach reduces the computational requirements while yielding fairly accurate trends. The results for straight burn discharge burnup and cycle length are provided in Figure 27 and Figure 28 respectively. Results for original design are provided by a line and

proposed design are provided by a respective line colour marker. Following observations can be made from both plots:

- In most cases, higher pitch results in higher burnup and longer cycle length. However, for cases (CHM > 250) with pitch 65 cm results in less efficient fuel utilization. Even though the moderation is increased in the core due to relatively more graphite content, the core leakage outweighs the increased system absorption. The discharge burnup and hence fuel utilization clearly has an optimum.

- The discharged time is decreased with increasing the CHM ratio. This can be attributed to having less fuel in the core. To eliminate frequent fuel reloading, and reduce outage costs, CHM must be optimized.

- Higher pitch ($> 55\ cm$) provides higher spectral shift benefits compared to original design. This is a result of neutrons being locally captured in ^{238}U during early periods.

If the primary objective of the design is to improve the fuel utilization, the optimum CHM ratio must be identified. The results presented here show that the proposed design performs better than the original design and that the optimum point is near CHM of 200.
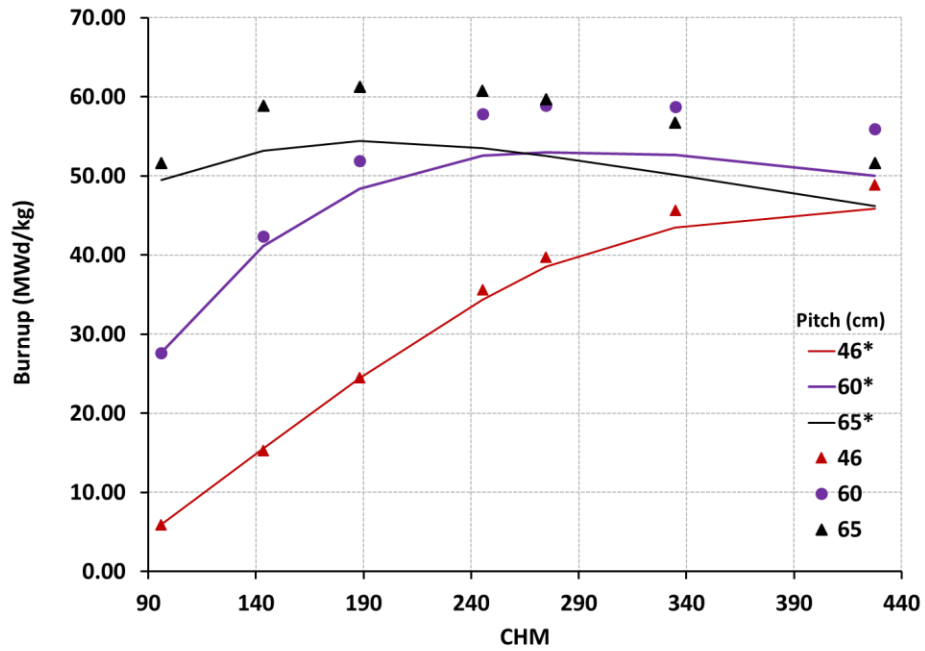
Figure 27 – Straight burn discharge burnup for original (*) and proposed design
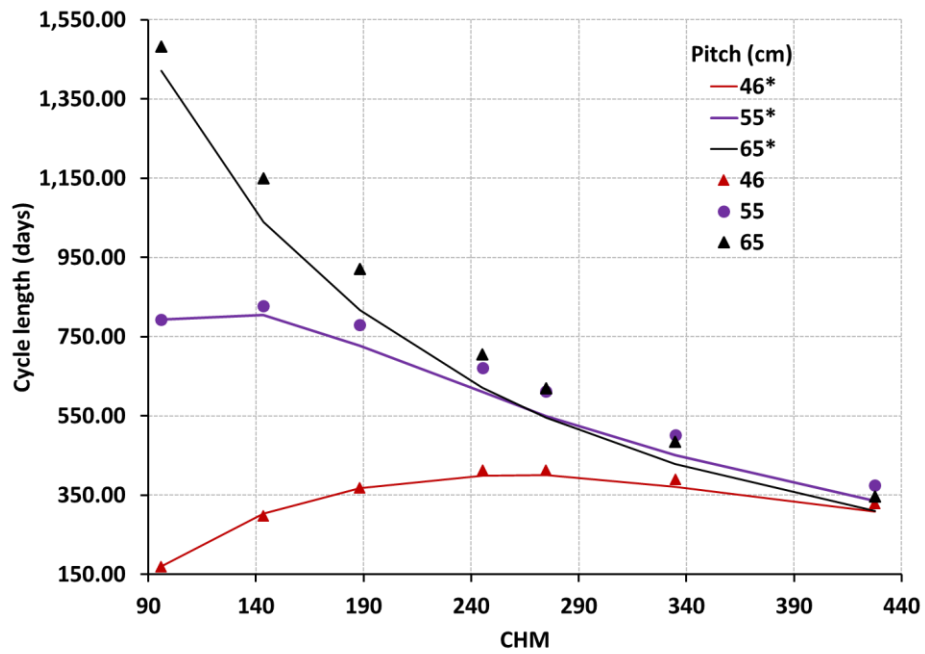
Figure 28 – Cycle length performance for original (*) and proposed design

Using the lessons learnt from above study, the second calculation stage relied on performing fine sensitivity studies near the optimum point (i.e. CHM of 200 and pitch of 60 cm) in order to identify the benefits of using the spectral shift operational regime. The sensitivity studies relied on varying the CHM ratio (170-250) and pitch (55-65). In addition, the analyses were extended to include the variation of PF (30-50%) and enrichment (5-19.75%). The sensitivity results are presented in Figure 29. The following trends can be observed:

- Increased enrichment provides better fuel utilization and cycle length. As an example, the fuel burnup does not exceed 30 MWd/kg, when 5% enriched fuel is used. However, the burnup values for 8% and 19.75% enrichments can reach burnups above 60 and 180 MWd/kg respectively.

- Increasing the pitch yields prolonged discharge burnup and cycle length.

- Increasing the CHM improves the fuel utilization since more moderation is available, however it decreases the cycle length significantly due to the reduced fissile content.

- Increasing the PF provides better cycle length due to the availability of more uranium although there is an optimum value for burnup.
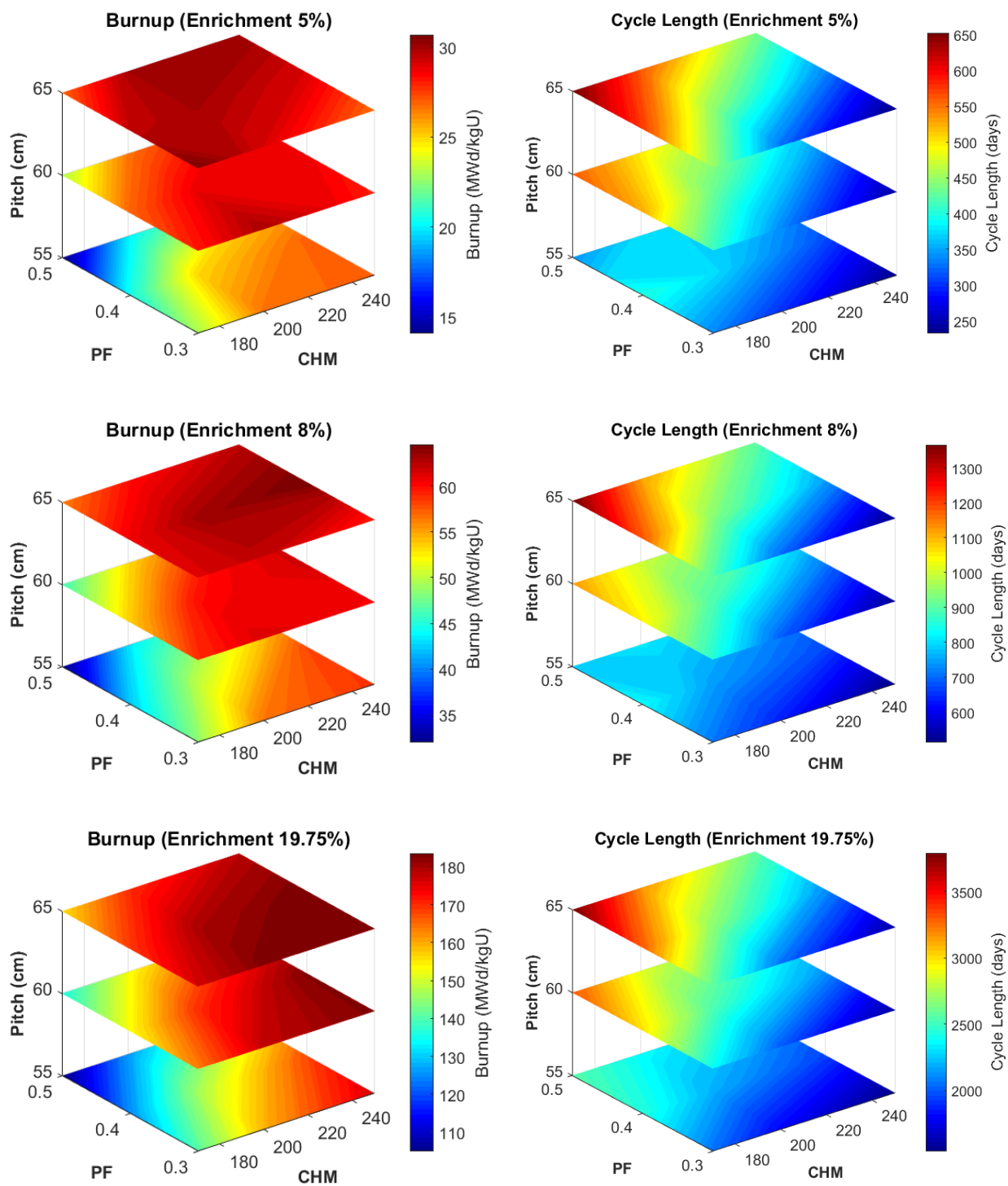
Figure 29 – Spectral shift sensitivity results

4.1.3 Comparison of Proposed vs Original Design

Although, increasing the enrichment to 19.75% clearly improves the benefits of using the spectral shift control mechanism, it was decided to limit the current analysis to 8%, as was done in the original study. For this enrichment, the maximum discharge burnup is obtained using a pitch of 65 cm and PF of 40%, whereas the original design used a pitch of 60 cm and PF of 40% [11]. As mentioned earlier, higher CHM provides higher burnup and lower cycle length.

The criticality curves for both designs are presented in Figure 30. The proposed design obtains a cycle length of 926 $days$ compared to 744 $days$ in the original case. The criticality in the proposed designed is maintained by continuously inserting the moderating elements into the core. The increased cycle length is achieved due to the accumulated ^{239}Pu in the system as shown in Figure 31. Inserting the moderating elements into the core allows to use the excess ^{239}Pu and obtain longer operation periods.

Note that the proposed design is already within the operational region limits. There is no excess reactivity that needs to be suppressed during the whole core cycle and therefore this design eliminates the need of burnable poison during its operation. Including the burnable poison consideration in the original design, maximum cycle length of 702 $days$ was achieved. The cycle length for burnable poison consideration can be compared with the spectral shift design in Figure 32. The burn cycle for spectral shift method is 224 $days$ longer than that of original design when burnable poison is considered. This is equivalent to discharge burnup gain of >30%.
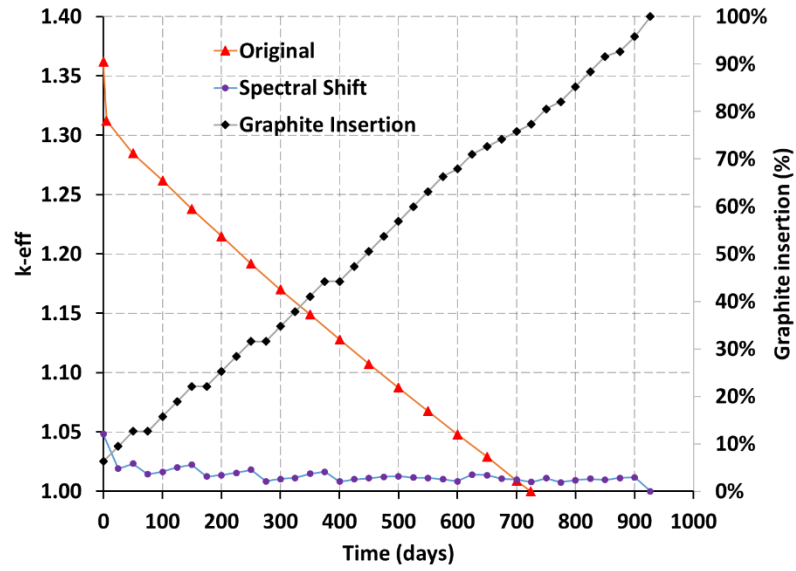
Figure 30 – K$_{eff}$ as a function of time for both original and spectral shift case
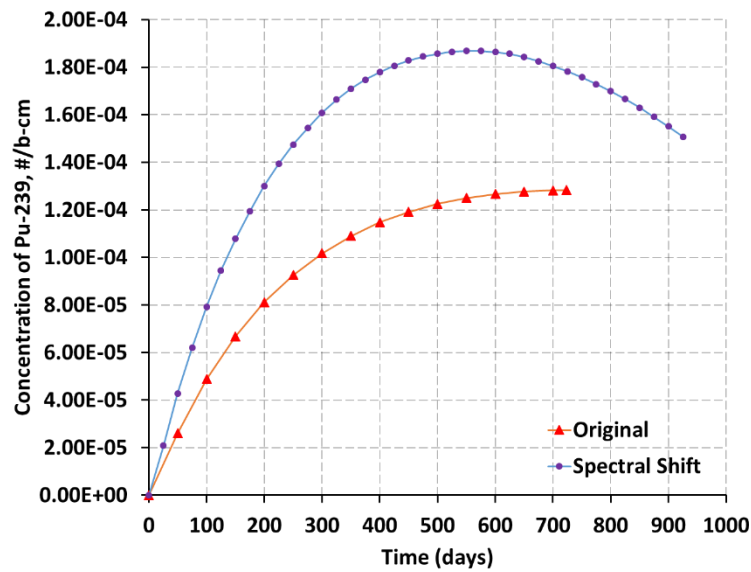
Figure 31 – ^{239}Pu concentration for the original and the spectral shift cases
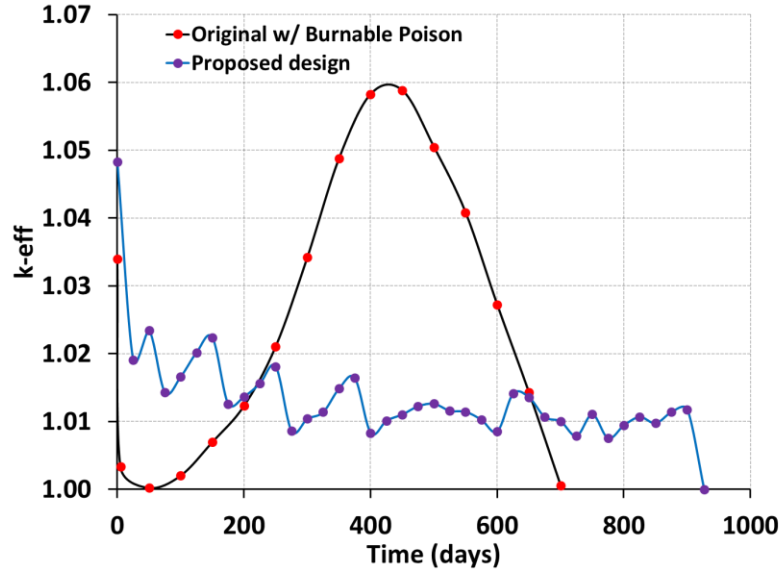
Figure 32 – Comparison of original design with burnable poison and spectral shift

4.1.4   Multibatch regime

For the original design, Linear Reactivity Model (LRM) was used to to estimate the discharge time. Using the multibatch geometries in Figure 12, equilibrium cycles for original and proposed design for 3-batch and 6-batch system are presented in Figure 33 and Figure 34 respectively.
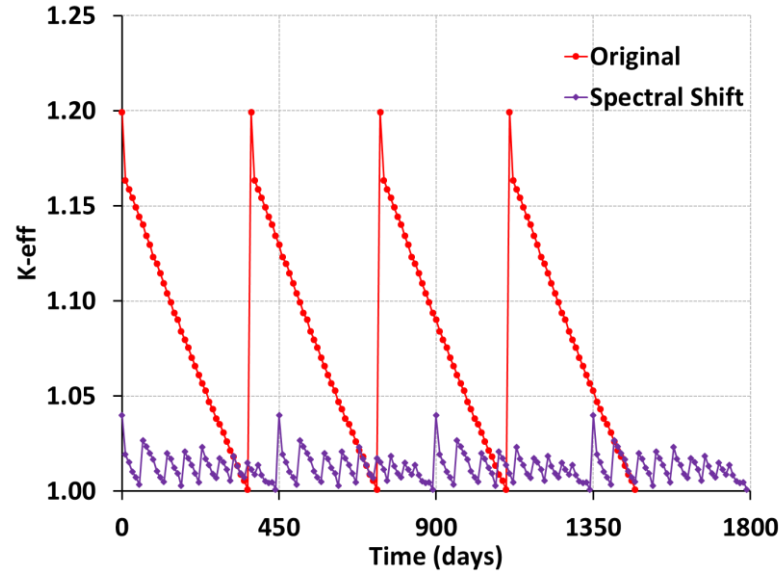
Figure 33 – k$_{eff}$ for 4 consecutive cycles with 3-batch system
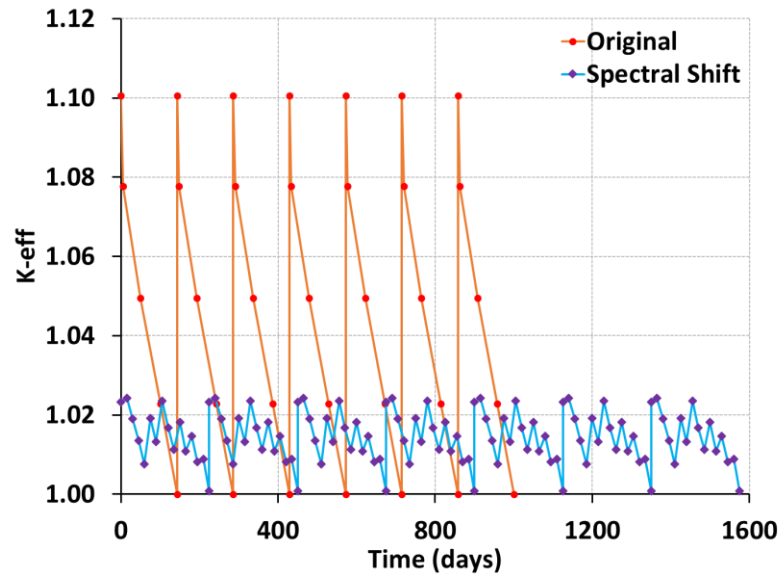
Figure 34 – k$_{eff}$ for 7 consecutive cycles with 6-batch system

The discharge time for both the original and proposed cases are provided in Figure 35. As expected, the benefit of using the spectral shift operation regime reduces with the number of batches. Without the burnable poison considerations for original multibatch design, spectral shift percent gain reduces from ~25% for 1-batch to ~10% for 6-batch system.
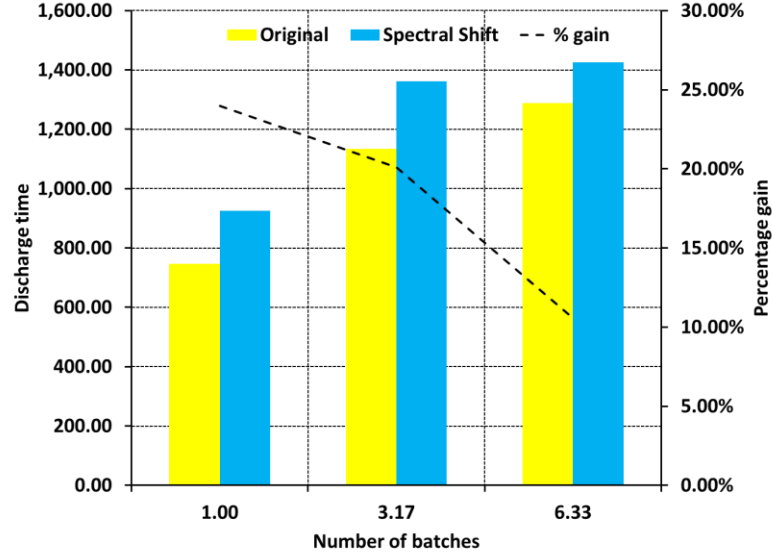
Figure 35 – Discharge time for original and spectral shift cases

4.1.5   Reactivity Coefficients

Reactivity coefficients are important safety parameters for examining accident scenarios. The reactivity coefficients for the original and proposed design were found using the following equations:

$$f = \frac{\partial \rho}{\partial T} = \frac{k_{per} - k_{reff}}{k_{per} \times k_{ref} \times (T_{per} - T_{ref})} \times 10^5 \left[\frac{pcm}{°C}\right]$$

$$\Delta f = \left[\left(\frac{\partial f}{\partial k_{per}}\right)^2 \Delta k_{per}^2 + \left(\frac{\partial f}{\partial k_{ref}}\right)^2 \Delta k_{ref}^2\right]^{\frac{1}{2}} \left[\frac{pcm}{°C}\right]$$

(21)

where f is the temperature coefficient, ρ is the reactivity, T is the temperature, k_{ref} and T_{ref} are reference criticality and temperature, k_{per} and T_{per} are the perturbed criticality and temperature, and Δf is the error. For the fuel and moderator, temperature points of 1200 K and 900 K, and for the coolant, temperature points of 900 K and 1200 K were used.

59

The values obtained for coefficients for 1-batch, 3-batch, and 6-batch refueling strategies are given in Table 4-1.

Table 4-1 – Reactivity Coefficients in $pcm/°K$ ($\pm\ error$)

The first row and second row represent the coefficients for the original and the proposed designs respectively.

		Fuel	Moderator	Coolant
1-batch	**BOL**	−2.370±0.097	+0.031±0.109	−0.664±0.089
		−5.583±0.167	−0.408±0.153	−1.229±0.194
	EOL	−3.641±0.183	−0.065±0.164	−0.314±0.189
		−3.215±0.135	−0.099±0.084	−0.375±0.098
3-batches	**BOL**	−2.526±0.098	−0.008±0.097	+0.120±0.080
		−4.618±0.109	+0.041±0.098	−0.345±0.118
	EOL	−3.403±0.125	+0.020±0.132	+0.562±0.121
		−3.210±0.095	+0.017±0.115	+0.468±0.098
6-batches	**BOL**	−2.872±0.112	+0.026±0.096	+0.150±0.098
		−3.791±0.111	+0.021±0.109	−0.113±0.096
	EOL	−3.199±0.102	+0.047±0.087	+0.391±0.088
		−3.152±0.107	+0.078±0.119	+0.517±0.103

In general, the reactivity coefficients were more negative in the proposed design compared to the original design. Following deductions can be made from the above three tables:

- The overall reactivity coefficients ($i.e.\ f_{fuel} + f_{mod.} + f_{cool.}$) for both original and proposed designs for all batches are always significantly negative.

- Greatest magnitude of negative Doppler coefficient is provided by fuel heating.

- At the BOL, the proposed regime provides significantly more negative overall coefficients, but towards EOL, the reactivity coefficients have similar values.

- For both designs, fuel temperature coefficients become more negative as we increase the number of batches. This is a direct result of the softer spectrum.

- The moderator temperature coefficient at BOL and EOL for both proposed and original designs is close to zero and becomes slightly positive as the number of batches are increased. However, the statistical uncertainty associated with this coefficient is considerably larger than the absolute value.

- The coolant coefficient is more negative for the proposed design than the original design. However, for both cases, the coefficient becomes eventually positive due to the build-up of plutonium. Yet, these values are considerably lower in magnitude compared to the fuel coefficients.

4.2   Thermal-Hydraulic Results

Full 3D core T/H calculations were performed for both the reference and the proposed cases at BOL only for the single batch cases. A 60° core symmetry was used to model only 4 representative T/H fuel assemblies, each subdivided to six T/H channels, as shown in Figure 36. Each T/H channel was modeled as the fuel meat within a graphite sleeve, surrounded by the coolant. There are total of 24 T/H channels, each divided into twenty equal-length axial regions, which resulted in 480 T/H regions in total.

a. Core radial T/H channels.   b. Sub-channels (T/H) within each assembly.
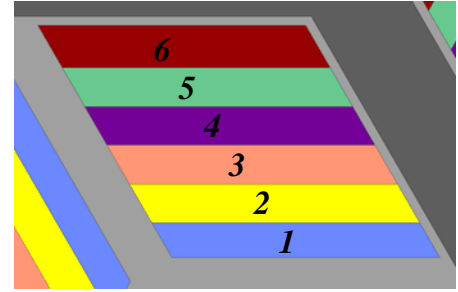
Figure 36 – Full core T/H model

Serpent was used to find the spatial power distribution. The statistical data was adjusted to produce power uncertainties below 1%. Serpent allows to generate mesh plots, in which the neutron moderation and fission power production can be illustrated. The BOL radial power distribution (through the mesh plot) is shown in Figure 37 for the original, and for the proposed design. The red and yellow shades represent relative fission power and the blue shade represents relative thermal flux.   Figure 37a shows sharp hot and cold color gradient along the radial geometry. This implies that the original design has a larger fission rate and thermal flux gradient in the core, hence larger power peaking. On the contrary, the proposed design has a lower power gradient within the core. Having less moderation at BOL flattens the power. Although, as the proposed system is becoming more and more "original" as we approach the EOL, it is expected that both designs will have similar power variation.
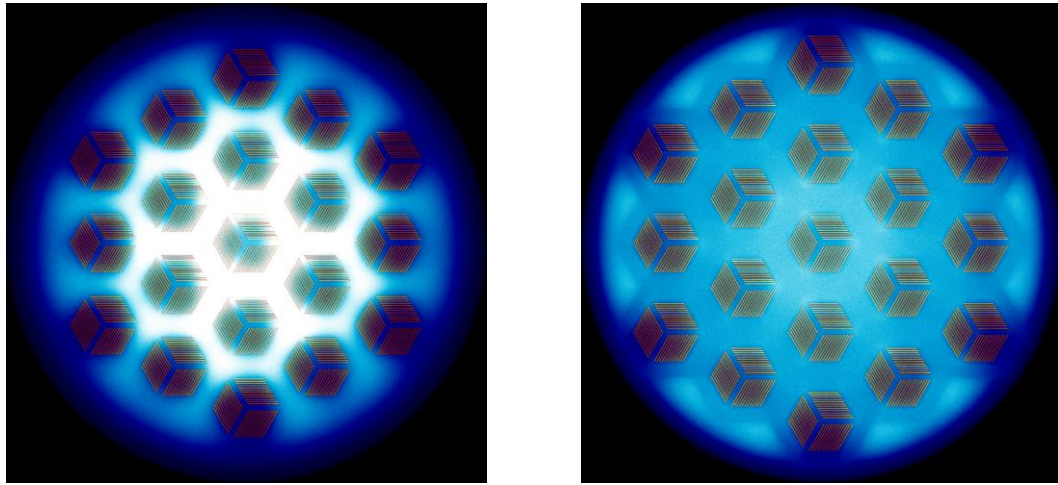
a. Original design   *b. Proposed design*

Figure 37 – BOL radial power mesh plots for both designs

This power distribution was used in THERMO to calculate the temperature and density distributions. The proposed design experiences harder spectrum compared to the original one at BOL. Therefore, the increased mean free path of the neutrons flattens the axial and radial power distributions, as shown in Figure 38 and Figure 39 respectively. Radial power peaking values are presented in Figure 39a for both the original and the proposed design. The total power peaking value for the original case was found to be 2.30, whereas the proposed design experiences a considerably lower power peaking value of 1.37 (-40%). The lower power peaking values results in a decrease of the fuel center line fuel temperature (Figure 39b) and a flatter coolant outlet temperature (Figure 39c). Both designs, however, are well within the T/H safety limits. Further coupled neutronic-T/H depletion studies must be performed to ensure that the proposed design with a movable graphite structure satisfies the imposed design limits. More specifically, it is necessary to investigate the core configurations with partial insertion of the movable graphite structure.
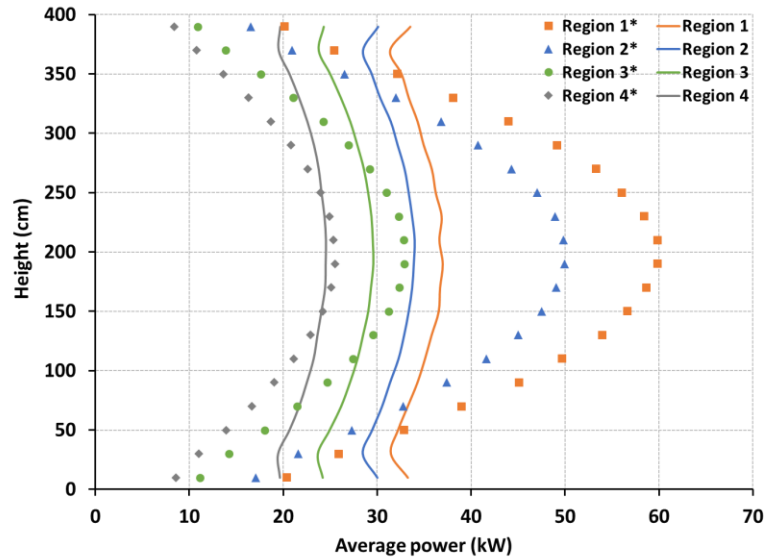
Figure 38 – Axial power distribution (plates' average) at BOL for the original (*) and the proposed designs.

| a. Power Peaking | b. Max centerline fuel temperature (^{0}C) | c. Coolant outlet temperature (^{0}C) |
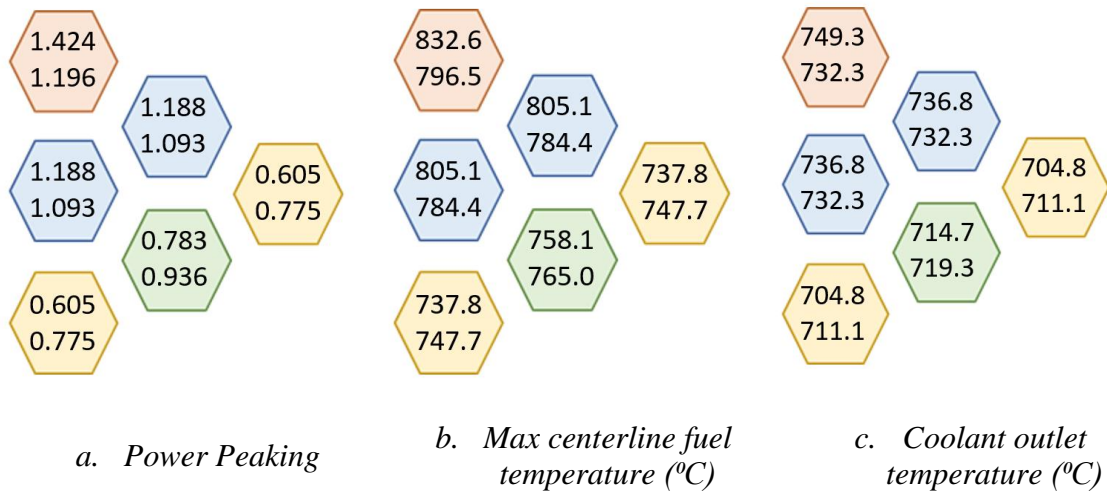
Figure 39 – Radial averaged T/H properties distributions. Original (top quantity) and Proposed (bottom quantity) design.

As previously mentioned, the T/H calculation sequence relied on an iterative scheme according to which the mass flow rate distribution is adjusted to satisfy a uniform pressure drop distribution. The mass flow rate values are presented in Figure 40 and the estimated pressure drop is $86\ kPa$.
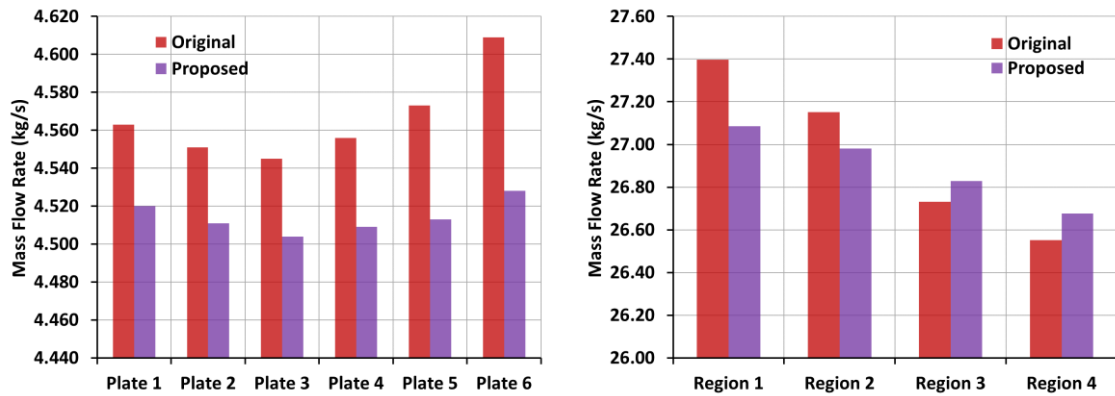
Figure 40 - Mass flow rate values in hottest fuel assembly (left) and for each region (right) for the original (maroon) and the proposed (purple) designs

Figure 41 and Figure 42 show the local (*i.e.* plate-wise) fuel center-line and coolant outlet temperatures respectively. It can be clearly seen that the proposed design experiences a lower power peaking within the assembly and thus outperforms the original design in respect to T/H safety margins. Both designs experience higher power peaking in plate 6, which is positioned on the periphery next to a graphite moderator.
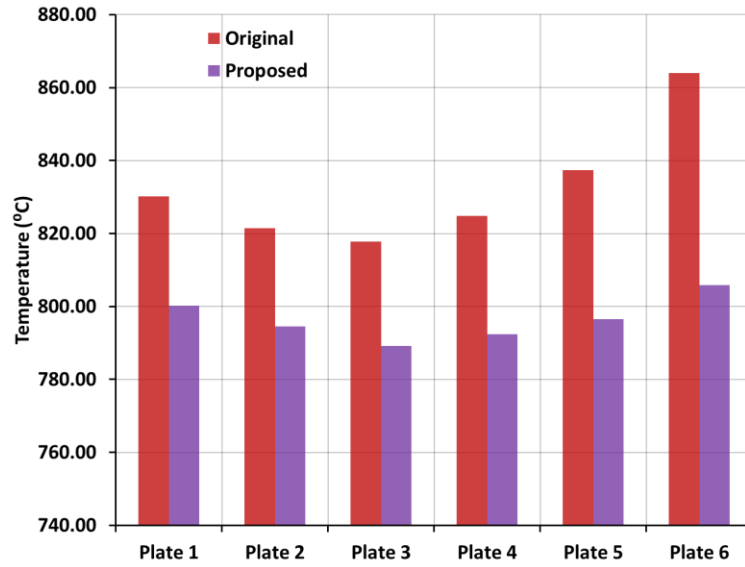
Figure 41 – Centerline temperature (⁰C) in each plate for the hottest assembly
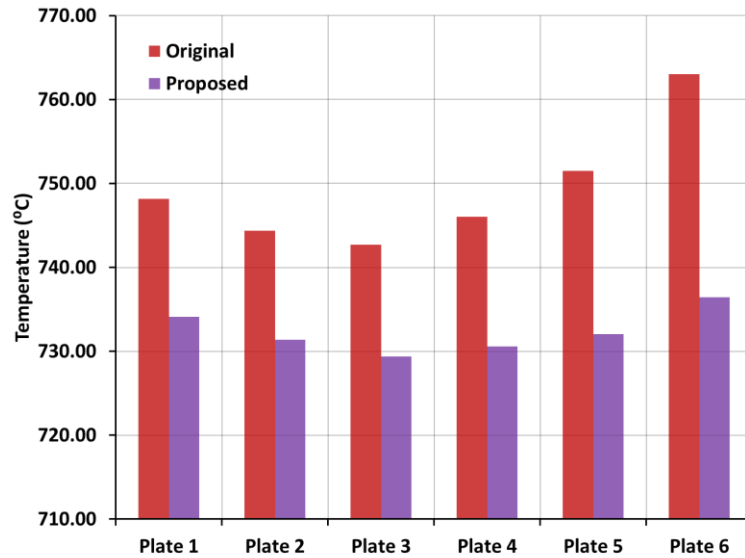
Figure 42 – Coolant outlet temperature (⁰C) in each channel for the hottest assembly

4.3 Fuel Cycle Costs

To estimate the fuel cycle gain using the spectral shift approach, a simplified economic model was used. In this model, the cost associated with the practical machinery required for spectral shift control were disregarded in this study. Additionally, inflation was ignored in this model. The fuel cycle model relied on the cost of U_3O_8 per kg, the conversion costs to UF_6 per kg, and the Separative Work Unit (SWU). The values for each costs were retrieved from the Ux consulting company (UxC) website [38] and are based on the Month-End prices of December 2017. The UF_6 conversion factor (f_S) provided by UxC website was 2.61285. These prices are reported in Table 4-2.

Table 4-2 – UxC prices for economic analysis

Symbol	Product	Price
P_U	U_3O_8, kg	$62.79
P_C	Conversion Price (kgU)	$4.60
P_S	SWU Price (kgU)	$39.00

The separation potential $V(x_i)$ for product ($x_p = 0.08$), waste ($x_w = 0.0025$), and feed ($x_f = 0.00711$) were calculated by Equation **22**.

$$V(x_i) = (2x_i - 1) \cdot ln\frac{x_i}{1 - x_i} \tag{22}$$

The feed factor (Equation **23**) and the waste factor (Equation **24**) were then evaluated.

$$\frac{F}{P} = \frac{x_p - x_w}{x_f - x_w} \tag{23}$$

$$\frac{W}{P} = \frac{F}{P} - 1 \tag{24}$$

The separation potential, the feed factor and waste factor were then used to calculate the SWU factor (Equation **25**) which describes the number of SWUs required per enriched kgU.

$$S = \frac{SWU}{P} = V(x_p) + \frac{W}{P} \cdot V(x_w) - \frac{F}{P} \cdot V(x_f) \tag{25}$$

The conversion and fabrication losses were neglected and the price (P_E) of enriched Uranium was calculated using (Equation **26**).

$$P_E = (P_U + P_C \cdot f_S) \cdot \frac{F}{P} + P_S \cdot S \tag{26}$$

The total cost (P_T) of the fuel per kgU was calculated by adding the fabrication costs (P_F) to the enrichment costs.

$$P_T = P_E + P_F \tag{27}$$

The TRISO particles fabrication costs have high uncertainties in prices due to the dependence of fabrication industry on further development. The estimated fabrication costs range from \$5,000 per kgU to \$30,000 per kgU with \$10,000 per kgU being the nominal cost [35].

To estimate the fuel costs and outage costs, in terms of \$/MWh_e, the cycle length (T_C), and discharge burnup (BU) with the thermal to electric conversion efficiency (η) of 40% were used as described in (Equation **28**) and (Equation **29**).

$$Fuel\ costs\left(\frac{\$}{MWh_e}\right) = \frac{Total\ cost\ of\ fuel}{BU \cdot \eta} \qquad (28)$$

$$Outage\ cost\left(\frac{\$}{MWh_e}\right) = \frac{Cost\ of\ outage}{Power \cdot T_C \cdot \eta} \qquad (29)$$

The fuel prices are described in Table 4-3.

Table 4-3 – Fuel Prices per kgU

Quantity	Value
S, SWU/kgU	14.42
$P_S \cdot S$, \$/kgU	562.34
P_E, \$/kgU	1,695.19
P_T, \$/kgU	11,695.19

The total fuel costs are reported in Table 4-4 for the different multi-batch schemes. In addition, the table presents the fuel cost for various fabrication costs (*i.e.* Low, Nominal, and High, which are chosen to be \$5,000/kgU, \$10,000/kgU, and \$30,000/kgU respectively).

Table 4-4 – Fuel costs for the proposed and original designs

	Cost type	Burnup (MWD/kg)		¢/$kWhe$	
		Original	Proposed	Original	Proposed
1 batch	Low			1.493	1.132
	Nominal	46.72	61.63	2.608	1.977
	High			7.067	5.357
3 batches	Low			0.947	0.769
	Nominal	73.63	90.72	1.655	1.343
	High			4.484	3.640
6 batches	Low			0.832	0.736
	Nominal	83.83	94.79	1.453	1.285
	High			3.938	3.483

The total outage costs for both original and proposed designs were found using Equation **29**. The outage costs were found by scaling the costs estimated for the AHTR design [21]. The scaling factor was found to be 27.2, which resulted in an outage costs of $0.83, $1.67 and $2.93 per $MWhe$ for a single-, three- and six- batches respectively. The total fuel costs (including outage) are presented in Table 4-5. Due to the extended cycle length and burnup provided by the spectral shift method, both the fuel costs, and outage costs for proposed design are lower than the costs for original design. It should be noted that the costs associated with burnable poison fabrications were not included in this analysis. Adding these costs, would further amplify the benefits of using the spectral shift method. Lastly, it must be emphasized that the costs associated with the practical control of the moderating elements were not analyzed here.

Table 4-5 – Fuel costs including outages for the proposed and original designs

	Cost type	Cycle length (*days*)		¢/*kWhe*		Savings %
		Original	Proposed	Original	Proposed	
1 batch	Low			1.576	1.195	
	Nominal	702	926	2.691	2.040	32
	High			7.150	5.420	
3 batches	Low			1.114	0.904	
	Nominal	349	430	1.822	1.479	23
	High			4.651	3.775	
6 batches	Low			1.125	0.995	
	Nominal	199	225	1.746	1.545	13
	High			4.231	3.743	

This FCC analysis was simplified using the optimized original and proposed design. However, it is recognized that depending on the chosen packing fraction, fuel and lithium enrichment, there would be large variations in the fuel cycle costs. These effects are studied in detail for the Liquid Salt Cooled Reactor [22]. For example, in their study, it was suggested that higher uranium enrichments are more economical than lower enrichments of 5% or below.

4.4 Extension of Spectral Shift Technique

There are several factors that should be considered for a practical spectral shift implementation in the SmAHTR design. These are listed below:

1. Spectral shift mechanism should be economically viable.

2. SmAHTR vessel dimensions must not vary upon this implementation.

3. During the steady-state moderator insertion event, the thermal performance must be within the safety limits.

4. Accident scenarios must be accounted for an event of inadvertent graphite insertion.

The above criteria were defined to validate that the spectral shift regime is in fact beneficial to the overall reactor design. Criteria 1 was set so that the design is profitable upon implementation. A design that is too costly would not be favoured to be implemented. Criteria 2 comes from the DOT requirements as described in Section 2.1. If the vessel dimensions are increased, then it would fail the United States DOT guidelines for a safe truck-trailer transportation. Hence, a method that does not require an increase in vessel height or width is needed. Criteria 3 accounts for the required thermal-hydraulic limits. It is expected that upon moderating element insertion, either from top or bottom, there will be a temporary power peaking at that location. Hence, a methodology must be developed for an axially uniform moderator insertion. Or on the other hand, it must be ascertained that the power peaking due to moderator insertion is inconsequential to the T/H limits. Criteria 4 ascertains that if the moderating element is accidentally inserted, then the core operation must continue safely, or sufficient shutdown margins are provided to overcome the positive reactivity insertion. If the graphite structures were inserted from top, then there is a probability of their accidental insertion/drop in the core during reactor-cycle.

Preliminary design suggests that the graphite structures would be removed and inserted in a similar pattern as described in Section 3.3.2. Such a design is realistic for a larger scaled FHR. However, for SmAHTR, based on the criteria set above, it is very difficult to remove graphite structures and axially store them without extending vessel height. Furthermore, holding these large graphite structures, let alone precise insertion, is

impractical. Moderator insertion will lead to power peaking at the edges. Structure based design would fail most of the criteria set above. Therefore, it is recognized that some other mechanism must be employed to provide spectral shift effect during reactor life. To do so, following design is proposed to be investigated in future studies.

The concept behind Pebble-Bed Fluoride High-temperature Reactors (PB-FHRs) is based on the pebbles having lower density than FLiBe, which allows their graphite pebbles and fuel pebbles to be buoyant and thus float upwards in FLiBe [5]. A similar concept is identified in this study. Alternative to graphite pebbles, graphite in powdered or dust form, is used in conjunction with beryllium fluoride (BeF_2), rather than FLiBe. Graphite having lower density than BeF_2 will float upwards in molten BeF_2. Therefore, it is envisioned that the external graphite structures from the core are removed, and instead the moderation through-out the core cycle is instead initially provided by BeF_2 and then through the insertion of graphite powder in BeF_2. A diagram representing such a paradigm is shown in Figure 43. At the BOL, no moderation is needed and hence the core will experience harder spectrum. BeF_2 being in a liquid state could be then introduced with a fractional density, enough to maintain reactor critical. The density of BeF_2 is then increased until its maximum density is achieved. After then, fractional amount of graphite is inserted in the liquid BeF_2 from the bottom of the core. Graphite having lower density will continuously float upwards which can be recirculated through a channel to the bottom of the core. The amount of this graphite is then continuously increased until the packing fraction of 70% is reached. Since graphite is in powder form, around 70% packing fraction is assumed to be achievable. Note that the implementation to investigate such an operation included inserting the graphite

dust while adjusting the amount of BeF_2 accordingly. MATLAB coupled BeF_2 spectral shift routine is shown in Figure 44.
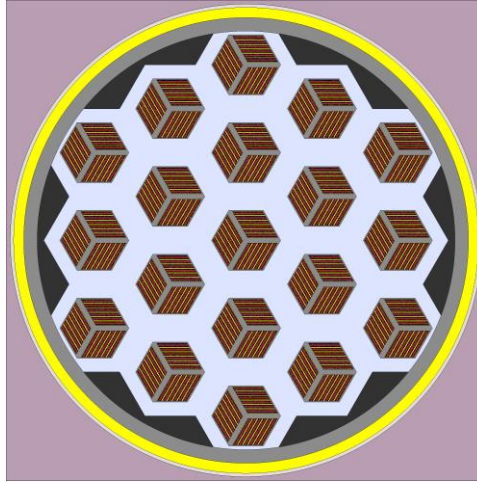
Figure 43 – BeF₂ utilized spectral shift

It is envisioned that such or similar to this design could be practically implemented in any smaller scale reactors like SmAHTR with relatively low capital investment overheads. Since the moderation is provided by this molten BeF_2, in an accident scenario, reactor could be turned subcritical by stopping its flow.
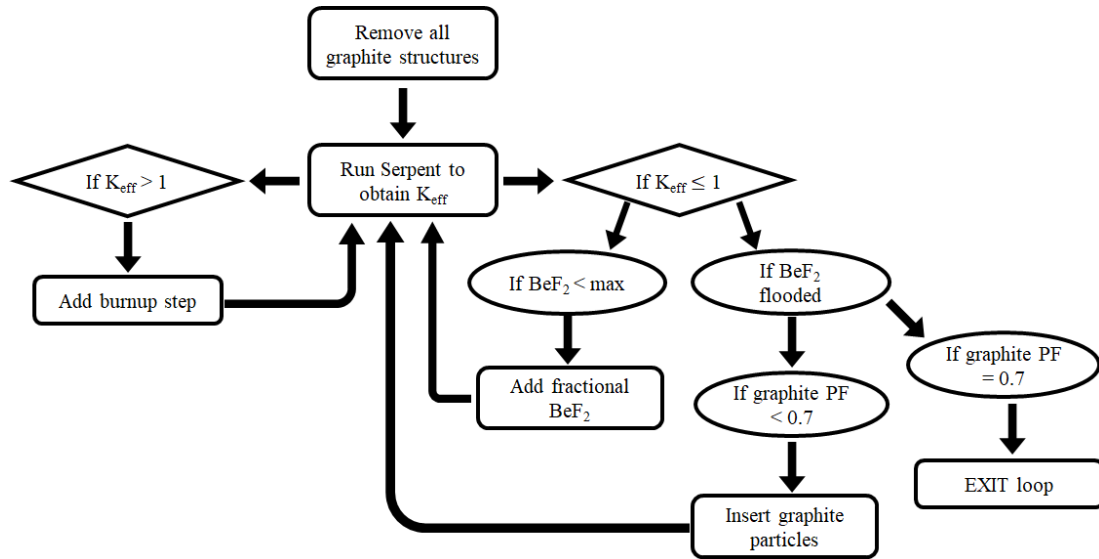
Figure 44 – Spectral shift routine with molten BeF₂

The criticality vs cycle length for a liquid BeF_2 based straight-burn concept is shown in Figure 45 (in red). Since beryllium is a good moderator, the reactivity can solely be controlled by molten BeF_2 until $675\ days$. After then, graphite particles are inserted fractionally into the system until the end of cycle $i.e.$ $830\ days$. The graphite structure based spectral shift provided $926\ days$ of fuel cycle. It is presumed that the ~100 $days$ cycle loss observed in this concept is due to combination of (i) not letting graphite packing fraction reach 100%, and (ii) BeF_2 incapable of reflecting as many neutrons as graphite back into the system. Therefore, another concept with BeO reflector was incorporated. In this concept, BeO is placed on the outer periphery of the core graphite to provide better neutron reflection. Using BeO as reflector, a cycle length of $875\ days$ was achieved (in purple). Further studies are needed to provide a mechanism to mount the fuel assemblies. In addition, the actual mechanism to control the fractional mass of BeF_2 should be envisioned. However, such a spectral shift implementation would eliminate some of the concerns associated with inserting graphite structure, such as local power peaking.

Additional coupled neutronics-T/H analysis must be performed to estimate the viability of such a scheme.
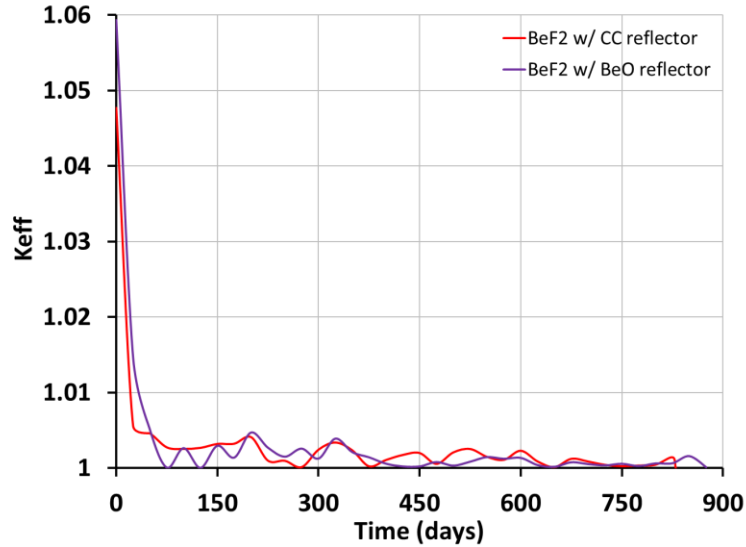
Figure 45 – Criticality vs time for a BeF₂ based concept

Although this study focused on the SmAHTR reactor concept, it is no longer a front-runner, due to the relatively long estimated time to deployment ([34], [30]). In spite this fact, it must be noted that the approach and results from this study could easily be extended to other FHR reactors such as, the Kairos PB-FHR [5] that was developed to enhance natural resource utilization due to its fuel management scheme. Additional example is the small $100\ MWt$ demonstration reactor, FHR-DR ([2], [31]), which utilizes the existing advanced gas reactor fuel and is designed to be deployable in the near-term future. Moreover, the current study considered a very specific spectral shift management, however, similar operational scheme can be adopted for liquid fueled and fluoride salts reactors ([1]). To conclude, the proposed spectral shift control, designated to extend burnup without reducing the cycle length and eliminate the need of burnable absorbers, is an attractive option to any FHR which employs graphite-based moderator.

CHAPTER 5.   SUMMARY AND FUTURE WORK

FHRs are attractive due to their high temperature output and safer due to their inherent passive decay heat removal. The use of TRISO fuel allows fission products to be accumulated in the layers, hence making this type of fuel more accident tolerant. However, fuel fabrication costs of TRISO based fuel used in FHRs is considerably more expensive than the cost of UO_2 fuel pellets. Therefore, the corresponding fuel cycle costs are economically less attractive.

To remedy the cost issue, we have investigated an alternative technique that relies on varying the core spectrum; hence the spectral shift name. Such an operational approach can increase both the cycle length and the burnup of FHRs simultaneously. To study this concept, the core was modeled with movable graphite structures. More specifically, at the BOL, a significant portion of graphite is removed from the reactor core. This provides less moderation in the reactor making the excess neutrons to be captured in the resonance region of ^{238}U breeding ^{239}Pu. Towards the EOL, graphite is continuously inserted into the reactor core maintaining criticality while burning the excess plutonium. The overall benefit of such an approach is expressed in an increase of both cycle length and burnup. Moreover, since the criticality is control via moderating elements, the proposed design requires no burnable poison.

Multiple sensitivity studies were performed here to identify the optimum design set. The objective function was chosen to be the burnup. It was found that an assembly pitch of $65\ cm$, and CHM of 200, and PF of 40% are most suitable for extending the burnup. The results indicated that a ~32% improvement can be achieved compared to the

SmAHTR-CTC design, which was used here as a reference case. To properly compare the proposed against the reference design, our studies included investigation of using different burnable poison options. The main objective was to identify the cycle penalty, due to the incomplete incineration of the burnable material, in the original case. Various multi-batch refueling strategies were also considered here as a way to improve the fuel utilization in both the original as well as the proposed design. As expected, the net gain of using the spectral shift regime decreases with the number of batches. Although, transient analyses were not conducted here, the reactivity coefficients for the proposed case were compared to the original ones. Comparable values with slightly more negative Doppler coefficients were observed. Safety margins were evaluated by performing T/H analysis at BOL for both cases. The proposed design outperforms the original one in respect to steady-state temperature distributions. Finally, this thesis presented economic studies to identify the cost savings for different refueling strategies and fabrication costs. The results indicate that a 32% improvement in cycle length amounts to $0.651 \text{ }¢/kWhe$.

Future studies could investigate the optimized insertion sequence and the corresponding axial spatial effects. Safety analyses associated with inadvertent insertion of moderating elements could/should also be considered. Controlled structure-based design could be implemented for a larger scale FHR using similar graphite sized rods as control rods. In this manner, no new mechanism needs to be developed since graphite rod could be inserted in a similar manner as a control rod. For a larger scale FHR, since space is less of an issue, these rods could be inserted from bottom of the reactor to prevent any accidental insertion. However, for a smaller scaled FHR like SmAHTR, due to its compact and transportable design, it is recognized that liquid based moderating element insertion would

be the most viable option. Therefore, further neutronic and T/H sensitivity studies needs to be investigated using different materials and different support mechanisms for this hexagonal or other fuel based SmAHTR design. Transient analysis must account for pump failure that may cause BeF_2 loss and subsequently re-insertion of graphite pebbles into the core giving a rise to reactivity. Detailed studies must be performed to account for economic and mechanical viability of using two fluids i.e. FLiBe and BeF_2 in the same core. Additional challenge is the higher pumping power requirements associated with the secondary molten moderator that reduces the thermodynamic efficiency. Lastly, material survivability caused by radiation damage due to the harder spectrum must be carefully examined.

APPENDIX A. SAMPLE SERPENT INPUT FILE

```
% ********************************************************
% ****************    Input for SmAHTR      *****************
% ********************************************************

set title "SOLID HEX TRISO PIN"

%--------------------------------------------------------
%  UCO TRISO fuel kernel enriched to 8.0% wt%
%--------------------------------------------------------

% --- FUEL TYPE 1 --- %
particle 80001
fuel1            0.02135
buffer           0.03135
IPyC             0.03485
SiC              0.03835
OPyC             0.04235
matrix1

% --- Explicit method
pbed 100001 77001 "disp40part1.inp"

cell 11001 77001 matrix1 -5001
surf 5001  inf

% --- FUEL TYPE 2 --- %
particle 80002
fuel2            0.02135
buffer           0.03135
IPyC             0.03485
SiC              0.03835
OPyC             0.04235
matrix1

% --- Explicit method
pbed 100002 77002 "disp40part2.inp"
cell 11002 77002 matrix1 -5002
surf 5002  inf

% --- FUEL TYPE 3 --- %
particle 80003
fuel3            0.02135
buffer           0.03135
IPyC             0.03485
SiC              0.03835
OPyC             0.04235
matrix1
```

```
% --- Explicit method
pbed 100003 77003 "disp40part3.inp"

cell 11003 77003 matrix1 -5003
surf 5003  inf


%--------------------------------------------------------
%  Fuel assembly
%--------------------------------------------------------

surf 100 hexyc 0 0 22.25 %hexagon structure for fuel pin

surf 1 plane 1.73205 1 0 0   %tan(60) x + y = 0

surf 2 plane 1.73205 1 0 4   %tan(60) x + y = (2/(sin60)*(tan60)) = 2sec(60)

surf 3 plane 1.73205 1 0 42.9711

surf 4 plane 1.73205 1 0 45


surf 11 py 0
surf 12 py 2

surf 13 py 2.35
surf 14 py 2.45
surf 15 py 3.07
surf 16 py 4.19
surf 17 py 4.81
surf 18 py 4.91

surf 19 py 5.61
surf 20 py 5.71
surf 21 py 6.33
surf 22 py 7.45
surf 23 py 8.07
surf 24 py 8.17

surf 25 py 8.87
surf 26 py 8.97
surf 27 py 9.59
surf 28 py 10.71
surf 29 py 11.33
surf 30 py 11.43

surf 31 py 12.13
surf 32 py 12.23
surf 33 py 12.85
surf 34 py 13.97
surf 35 py 14.59
surf 36 py 14.69
```

```
surf 37 py 15.39
surf 38 py 15.49
surf 39 py 16.11
surf 40 py 17.23
surf 41 py 17.85
surf 42 py 17.95

surf 43 py 18.65
surf 44 py 18.75
surf 45 py 19.37
surf 46 py 20.49
surf 47 py 21.11
surf 48 py 21.21

surf 89 py 21.5
surf 90 py 22.5

cell a01 1 coolant 2 -3 12 -13

cell a11 1 sleeve    2 -3 13 -14
cell a21 1 fill 100001 2 -3 14 -15
cell a31 1 sleeve    2 -3 15 -16
cell a41 1 fill 100001 2 -3 16 -17
cell a51 1 sleeve    2 -3 17 -18

cell b01 1 coolant 2 -3 18 -19

cell b11 1 sleeve    2 -3 19 -20
cell b21 1 fill 100001 2 -3 20 -21
cell b31 1 sleeve    2 -3 21 -22
cell b41 1 fill 100001 2 -3 22 -23
cell b51 1 sleeve    2 -3 23 -24

cell c01 1 coolant 2 -3 24 -25

cell c11 1 sleeve    2 -3 25 -26
cell c21 1 fill 100001 2 -3 26 -27
cell c31 1 sleeve    2 -3 27 -28
cell c41 1 fill 100001 2 -3 28 -29
cell c51 1 sleeve    2 -3 29 -30

cell d01 1 coolant 2 -3 30 -31

cell d11 1 sleeve    2 -3 31 -32
cell d21 1 fill 100001 2 -3 32 -33
cell d31 1 sleeve    2 -3 33 -34
cell d41 1 fill 100001 2 -3 34 -35
cell d51 1 sleeve    2 -3 35 -36

cell e01 1 coolant 2 -3 36 -37

cell e11 1 sleeve    2 -3 37 -38
cell e21 1 fill 100001 2 -3 38 -39
```

```
cell e31 1 sleeve     2 -3 39 -40
cell e41 1 fill 100001 2 -3 40 -41
cell e51 1 sleeve     2 -3 41 -42

cell f01 1 coolant 2 -3 42 -43

cell f11 1 sleeve     2 -3 43 -44
cell f21 1 fill 100001 2 -3 44 -45
cell f31 1 sleeve     2 -3 45 -46
cell f41 1 fill 100001 2 -3 46 -47
cell f51 1 sleeve     2 -3 47 -48

cell g01 1 coolant 2 -3 48 -89

cell a02 2 coolant 2 -3 12 -13

cell a12 2 sleeve     2 -3 13 -14
cell a22 2 fill 100002 2 -3 14 -15
cell a32 2 sleeve     2 -3 15 -16
cell a42 2 fill 100002 2 -3 16 -17
cell a52 2 sleeve     2 -3 17 -18

cell b02 2 coolant 2 -3 18 -19

cell b12 2 sleeve     2 -3 19 -20
cell b22 2 fill 100002 2 -3 20 -21
cell b32 2 sleeve     2 -3 21 -22
cell b42 2 fill 100002 2 -3 22 -23
cell b52 2 sleeve     2 -3 23 -24

cell c02 2 coolant 2 -3 24 -25

cell c12 2 sleeve     2 -3 25 -26
cell c22 2 fill 100002 2 -3 26 -27
cell c32 2 sleeve     2 -3 27 -28
cell c42 2 fill 100002 2 -3 28 -29
cell c52 2 sleeve     2 -3 29 -30

cell d02 2 coolant 2 -3 30 -31

cell d12 2 sleeve     2 -3 31 -32
cell d22 2 fill 100002 2 -3 32 -33
cell d32 2 sleeve     2 -3 33 -34
cell d42 2 fill 100002 2 -3 34 -35
cell d52 2 sleeve     2 -3 35 -36

cell e02 2 coolant 2 -3 36 -37

cell e12 2 sleeve     2 -3 37 -38
cell e22 2 fill 100002 2 -3 38 -39
cell e32 2 sleeve     2 -3 39 -40
cell e42 2 fill 100002 2 -3 40 -41
cell e52 2 sleeve     2 -3 41 -42
```

cell f02 2 coolant 2 -3 42 -43

cell f12 2 sleeve   2 -3 43 -44
cell f22 2 fill 100002 2 -3 44 -45
cell f32 2 sleeve   2 -3 45 -46
cell f42 2 fill 100002 2 -3 46 -47
cell f52 2 sleeve   2 -3 47 -48

cell g02 2 coolant 2 -3 48 -89

cell a03 3 coolant 2 -3 12 -13

cell a13 3 sleeve   2 -3 13 -14
cell a23 3 fill 100003 2 -3 14 -15
cell a33 3 sleeve   2 -3 15 -16
cell a43 3 fill 100003 2 -3 16 -17
cell a53 3 sleeve   2 -3 17 -18

cell b03 3 coolant 2 -3 18 -19

cell b13 3 sleeve   2 -3 19 -20
cell b23 3 fill 100003 2 -3 20 -21
cell b33 3 sleeve   2 -3 21 -22
cell b43 3 fill 100003 2 -3 22 -23
cell b53 3 sleeve   2 -3 23 -24

cell c03 3 coolant 2 -3 24 -25

cell c13 3 sleeve   2 -3 25 -26
cell c23 3 fill 100003 2 -3 26 -27
cell c33 3 sleeve   2 -3 27 -28
cell c43 3 fill 100003 2 -3 28 -29
cell c53 3 sleeve   2 -3 29 -30

cell d03 3 coolant 2 -3 30 -31

cell d13 3 sleeve   2 -3 31 -32
cell d23 3 fill 100003 2 -3 32 -33
cell d33 3 sleeve   2 -3 33 -34
cell d43 3 fill 100003 2 -3 34 -35
cell d53 3 sleeve   2 -3 35 -36

cell e03 3 coolant 2 -3 36 -37

cell e13 3 sleeve   2 -3 37 -38
cell e23 3 fill 100003 2 -3 38 -39
cell e33 3 sleeve   2 -3 39 -40
cell e43 3 fill 100003 2 -3 40 -41
cell e53 3 sleeve   2 -3 41 -42

cell f03 3 coolant 2 -3 42 -43

```
cell f13 3 sleeve      2 -3 43 -44
cell f23 3 fill 100003 2 -3 44 -45
cell f33 3 sleeve      2 -3 45 -46
cell f43 3 fill 100003 2 -3 46 -47
cell f53 3 sleeve      2 -3 47 -48

cell g03 3 coolant 2 -3 48 -89


cell 1171 1 graphite 1 -2 11 -90
cell 1271 1 graphite 3 -4 11 -90
cell 1371 1 graphite 2 -3 89 -90
cell 1471 1 graphite 2 -3 11 -12

cell 2171 2 graphite 1 -2 11 -90
cell 2271 2 graphite 3 -4 11 -90
cell 2371 2 graphite 2 -3 89 -90
cell 2471 2 graphite 2 -3 11 -12

cell 3171 3 graphite 1 -2 11 -90
cell 3271 3 graphite 3 -4 11 -90
cell 3371 3 graphite 2 -3 89 -90
cell 3471 3 graphite 2 -3 11 -12

cell 671 1 graphite -1:4:-11:90
cell 672 2 graphite -1:4:-11:90
cell 673 3 graphite -1:4:-11:90

cell 61 1 graphite -1:4:-11:90
cell 62 2 graphite -1:4:-11:90
cell 63 3 graphite -1:4:-11:90

cell 991 7 fill 1 -100
cell 1001 7 Tie  100
cell 992 8 fill 2 -100
cell 1002 8 Tie  100
cell 993 9 fill 3 -100
cell 1003 9 Tie  100

set usym 1 3 3 0 0 0 120
set usym 2 3 3 0 0 0 120
set usym 3 3 3 0 0 0 120

lat 10  3  0.0 0.0 11 11 60
 5 5 5 5 5 5 5 5 5 5 5
  5 5 5 5 5 5 5 5 5 5 5
   5 5 5 5 5 5 5 5 5 5 5
    5 5 5 5 5 9 9 9 5 5 5
     5 5 5 5 9 8 8 9 5 5 5
      5 5 5 9 8 7 8 9 5 5 5
       5 5 5 9 8 8 9 5 5 5 5
        5 5 5 9 9 9 5 5 5 5 5
```

```
            5 5 5 5 5 5 5 5 5 5 5
              5 5 5 5 5 5 5 5 5 5 5
               5 5 5 5 5 5 5 5 5 5 5
```

pin 5
Tie

surf 150 cyl 0.0 0.0 163.00   % Outer diameter including Reflector
surf 160 cyl 0.0 0.0 164.00   % Inside of core barrel made of boron carbide
surf 170 cyl 0.0 0.0 165.00   % 2-cm-thick core barrel
surf 180 cyl 0.0 0.0 172.50   % Coolant outer
surf 190 cyl 0.0 0.0 175.00   % Vessel Hastelloy-N

surf 195 cuboid -178 178 -178 178 -0.2 0.2 % Dummy cell for boundary conditions

cell 200 11 fill   10 -150   % Inner core-inside barrel
cell 201 11 graphite 150 -160   % Barrel, Radial graphite blocks -> boron carbide
cell 202 11 graphite 160 -170
cell 203 11 coolant   170 -180   % Coolant
cell 204 11 hastelloy 180 -190   % Vessel
cell 205 11 dummy_mat 190

cell 996 0 fill 11 -195   % Outside world
cell 999 0 outside 195

%---
%   Fuel and material description
%---

% --- 3 region fuel
mat fuel1   sum vol 10.2121 rgb 255 153 204 burn 1
92235.12c   0.0019839
92238.12c   0.022527
 8016.12c   0.036766
 6000.12c   0.012255

mat fuel2   sum vol 61.2723 rgb 153 255 255 burn 1
92235.12c   0.0019839
92238.12c   0.022527
 8016.12c   0.036766
 6000.12c   0.012255

mat fuel3   sum vol 122.5446 rgb 255 102 102 burn 1
92235.12c   0.0019839
92238.12c   0.022527
 8016.12c   0.036766
 6000.12c   0.012255

% --- Dummy material for the boundary conditions

```
mat dummy_mat -0.00001 rgb 10 10 10
9019.09c    -0.00000000001   %F

mat borcarb -2.52 rgb 200 200 200
5010.09c  -1.44242E-01
5011.09c  -6.38368E-01
6000.09c  -2.17390E-01

% Vessel material
mat hastelloy -8.86 rgb 227 222 219
28000.12c -0.70
42000.12c -0.172
24000.12c -0.074
26000.12c -0.045
14000.12c -0.006

% ---- Buffer, IPyC, Silicon Carbide, OPyC, Matrix Material ----
mat buffer -1.00
6000.12c          5.0140E-2

mat IPyC -1.90
6000.12c          9.5265E-2

mat SiC -3.20
14000.12c          4.8062E-2          %Silicon
 6000.12c          4.8062E-2          %Carbon natural

mat OPyC -1.87
6000.12c          9.3761E-2

% --- matrix composition between TRISO particles
mat matrix1 -1.75 moder graph2 6000 rgb 189 81 210
6000.12c     7.9722E-2

mat trisolayer -1.91317013 tmp 1473.15 rgb 192 192 192
14000.12c   0.003755145   %Silicon
 6000.12c   0.076304410   %Carbon natural

% --- Fuel graphite central matrix
mat sleeve -1.75 tmp 1000 rgb 165 42 42
6000.09c          7.9722E-2

% --- assembly to assembly graphite
mat Tie -1.95  rgb 50 50 50
6000.09c          7.9722E-2

% --- Wall (channel box) and Y shape
mat graphite  -1.95 tmp 1000 moder graph1 6000 rgb 140 140 140
6000.09c          7.9722E-2

% --- void graphite
mat voidcc  -0.0000001 rgb 168 255 227
6000.09c          7.9722E-2
```

```
% --- Flibe  Coolant:
mat coolant -1.95 tmp 948.15 rgb 255 255 0   %T=700K for temperature dependent density
3007.09c    2.3721E-2   %Li7
3006.09c    1.3834E-6   %Li6
4009.09c    1.1861E-2   %Be
9019.09c    4.7444E-2   %F

% ---- Thermal scattering data for graphite ----
therm graph1 gre7.20t    %For 1000 K
therm graph2 gre7.22t    %For 1200 K

% --- Boundary condition:
set bc 1 1 3

% --- Neutron population and criticality cycles
set pop 20000 250 20

% --- print material compositions
%set printm 1

% --- Geometry and mesh plots:
plot 3 2000 2000
plot 3 3000 3000 0.0 -30 30 -30 30
mesh 3 500 500

% --- Cross section library file path:
set declib "/DATA/sss_endfb7.dec"
set nfylib "/DATA/sss_endfb7.nfy"
set acelib "/DATA/sss_endfb7u.xsdata"


% --- Reduce energy grid size

set egrid 5E-5 1E-9 15.0

% --- Cut-offs:
set fpcut   1E-6
set stabcut 1E-12


% --- Options for burnup calculation
set bumode  2  % CRAM method
set pcc     0  % Predictor-corrector calculation on60
set xscalc  2  % Cross sections from spectrum

set powdens 0.06655 %power density

% --- Nuclide inventory:
set inventory

% Actinides:
922350
```

922380
942390
942400
942410
942420
952410
952440
952450

% Fission products:
360850
380900
471101
551370
541350
621490
621510

dep daystep
5
45
50
50
50
50
50
50
50
50
50
50
50
50
50
50
50
50

REFERENCES

[1]   Betzler, B.R., Robertson, S., Davidson, E.E., Powers, J.J., Worrall, A., Dewan, L., Massie, M., 2018. Fuel cycle and neutronic performance of a spectral shift molten salt reactor design. Ann. Nucl. Energy 119, 396–410.

[2]   Brown, N.R., Betzler, B.R., Carbajo, J.J., Wysocki, A.J., Greenwood, M.S., Gentry, C. and Qualls, A.L., 2017. Preconceptual design of a fluoride high temperature salt-cooled engineering demonstration reactor: Core design and safety analysis. Annals of Nuclear Energy, 103, pp.49-59.

[3]   Cisneros, A., 2013. Pebble Bed Reactors Design Optimization Methods and their Application to the Pebble Bed Fluoride Salt Cooled High Temperature Reactor (PB-FHR). 859.

[4]   Driscoll M. J., Downar T. J. and Pilat E. E., 1990. The Linear Reactivity Model for Nuclear Fuel Management, American Nuclear Society, LaGrange Park, Illinois.

[5]   Fei, T., D. Ogata, K. Pham, M. Solom, C. Zhao, C. Xu, A. Cheng, et al. 2008. A Modular Pebble-Bed Advanced High Temperature Reactor. Berkeley: University of California, Berkeley.

[6]   Forsberg C.W., Peterson P.F., Pickard P.S., 2003. Molten-Salt-Cooled Advanced High-Temperature Reactor for Production of Hydrogen and Electricity, Nuclear Technology, 144:3, 289-302, DOI: 10.13182/NT03-1.

[7]   Forsberg, C.W., 2004. The Advanced High-Temperature Reactor: High-Temperature Fuel, Molten Salt Coolant, and Liquid-Metal Reactor Plant. 1st COE-INES Int. Symp. on Innovative Nuclear Energy Systems for Sustainable Development of the World.

[8]   Gentry, C., Maldonado, G., Chvala, O., & Petrovic, B. (2017). Neutronic Evaluation of a Liquid Salt–Cooled Reactor Assembly. Nuclear Science and Engineering, 187(2), 166-184.

[9]   Greene, S.R., 2010. Pre-Conceptual Design of a Fluoride-Salt-Cooled Small Modular Advanced High-Temperature Reactor (SmAHTR). Tennessee: ORNL/TM-201/199.

[10]   Ho, M. & Yeoh, G. & Braoudakis, G., 2013. Molten Salt Reactors, Materials and Processes for Energy: Communicating Current Research and Technological Developments, 761-768.

[11]   Ilas, D., Holcomb, D.E., Gehin, J.C., 2014. SmAHTR-CTC Neutronic Design. Proc Physor, Kyoto, Japan.

[12]   Ingersoll D. T. et al., May 2004. Status of Preconceptual Design of the Advanced High-Temperature Reactor (AHTR). ORNL/TM-2004/104.

[13]   Kerner E. H., 1955. The Electrical Conductivity of Composite Media. Proceedings of the Physical Society. Section B, 69, Number 8.

[14]   Kotlyar, D., Lindley, B., Mohamed, H., 2017. Improving fuel utilization in SmAHTR with spectral shift control design: proof of concept. Ann. Nucl. Energy 104, 53–63.

[15]   Kotlyar, D., Shaposhnik, Y., Fridman, E., Shwageraus, E., 2011. Coupled Neutronic Thermo-hydraulic Analysis of full PWR Core with Monte-Carlo Based BGCore System. Nuclear Engineering and Design, 241, pp. 3777–3786.

[16]   Leppänen, J. et al., 2015. The serpent Monte Carlo code: status, development and applications in 2013. Ann. Nucl. Energy 82, 142–150.

[17]   Leppänen, J., 2007. Development of a new Monte Carlo reactor physics code. D.Sc. Thesis, Helsinki University of Technology.

[18]   Leppänen, J., 2010. Performance of Woodcock delta-tracking in lattice physics applications using the Serpent Monte Carlo reactor physics burnup calculation code. Ann. Nucl. Energy 37, 715–722.

[19]   Leppänen, J., 2015. SERPENT a Continuous energy Monte Carlo Reactor Physics Burnup Calculation Code, VTT Technical Research Centre of Finland.

[20]   Lewis J.V., 1967. Estimating Thermal Conductivity of Cermet Fuel Materials for Nuclear Reactor Application. Lewis Research Center Cleveland, Ohio. Tech. Rep. NASA TN D-3898.

[21]   Lewis, S. M., Petrovic, B., Mechanical Engineering, Sjoden, G. E., Stacey, W. M., & Maldonado, G. I., 2014. Simplified Core Physics and Fuel Cycle Cost Model for Preliminary Evaluation of LSCR Fueling Options.

[22]   Lewis, S., & Petrovic, B. (2013). Simplified fuel cycle cost model applied to LCSR parametric studies. Transactions of the American Nuclear Society, 109(2), 1476-1479.

[23]   Mars, D., Gans, D., 1961. Spectral Shift Control Reactor Design and Economic Study, BAW-1241. Babcock & Wilcox Company.

[24]   Matsuo H., 2000. Measurements of Thermal Diffusivities of Fine-Grained Isotropic Graphites from Room temperature to 2000 C by Laser Flash Method. Netsu Sokutei, 17(1), 2-8.

[25]   Mehta, V., Kotlyar, D., 2017a. Use of Spectral Shift to Greatly Improved Uranium Utilization in FHR Designs. Transactions of the American Nuclear Society, San Francisco, California.

[26]   Mehta, V., Kotlyar, D., 2017b. Spectral Shift Operation with Multi-Reloading Scheme Analysis in the SmAHTR Design. Transactions of the American Nuclear Society, Washington, D.C.

[27]   Mehta, V., Kotlyar, D., 2018. Thermal Hydraulics Assessment of the SmAHTR Reactor under the Spectral Shift Operation. Transactions of the American Nuclear Society, Gainesville, FL.

[28]   Mehta, V., Kotlyar, D., 2019. Core analysis of spectral shift operated SmAHTR. Annals of Nuclear Energy, 123, 46-58.

[29]   Petrovic, B., Maldonado, G.I., 2016. Fuel and Core Design Options to Overcome the Heavy Metal Loading Limit and Improve Performance and Safety of Liquid Salt Cooled Reactors. DOE NEUP Project Report 12-3870.

[30]   Petti, D., Hill, R., Gehin, J., Gougar, H., Strydom, G., O'Connor, T., Heidet, F., Kinsey, J., Grandy, C., Qualls, A. and Brown, N., 2017. A Summary of the Department of Energy's Advanced Demonstration and Test Reactor Options Study. Nuclear Technology, 199(2), pp.111-128.

[31]   Qualls, A.L., Betzler, B.R., Brown, N.R., Carbajo, J.J., Greenwood, M.S., Hale, R., Harrison, T.J., Powers, J.J., Robb, K.R., Terrell, J. and Wysocki, A.J., 2017. Preconceptual design of a fluoride high temperature salt-cooled engineering demonstration reactor: Motivation and overview. Annals of Nuclear Energy, 107, pp.144-155.

[32]   Ronen, Y., Galperin, A., 1980. A comparison between spectral shift control methods for light water reactors. Ann. Nucl. Energy 7, 59–64.

[33]   Savvatimskiy A.I., Carbon at high temperatures P. 1-246. Springer Mater. Sci., 134 (2015), 10.1007/978-3-319-21350-7.

[34]   Scarlat, R.O., Laufer, M.R., Blandford, E.D., Zweibaum, N., Krumwiede, D.L., Cisneros, A.T., Andreades, C., Forsberg, C.W., Greenspan, E., Hu, L.W. and Peterson, P.F., 2014. Design and licensing strategies for the fluoride-salt-cooled, high-temperature reactor (FHR) technology. Progress in Nuclear Energy, 77, pp.406-420.

[35]   Shropshire, D.E. et al., 2009. Adv. Fuel Cycle Cost Basis. INL/EXT-07-12107.

[36]   Snead, L.L., Nozawa, T., Katoha, Y., Byuna, T., Kondo, S., Petti, D. A., 2007. Handbook of SiC properties for fuel performance modeling. Journal of Nuclear Materials, 371 (1-3), 329-377.

[37]   Sohal, M. S., Ebner, M. A., Sabharwall, P., Sharpe, P., 2012. Engineering Database of Liquid Salt Thermophysical and Thermochemical Properties (Technical report INL/EXT-10-18297). Idaho National Laboratory, Idaho Falls, Idaho.

[38]   The Ux Consulting Company, LLC, 2017.
        https://www.uxc.com/p/prices/UxCPrices.aspx

[39]   Varma, V.K. et al., 2012. AHTR Mechanical, Structural, and Neutronic Preconceptual Design ORNL/TM-2012/320. Oak Ridge National Laboratory, Oak Ridge, TN.

[40]   Williams, D. F. 2006. Assessment of Candidate Molten Salt Coolants for NGNP/NHI Heat Transfer Loop (Technical report ORNL/TM 2006/69). Oak Ridge National Laboratory, Oak Ridge, TN.

[41]   Yokomizo, O. et al., 1993. Spectral shift rod for the boiling water reactor. Nuclear Engineering and Design, 144(2), 223-236.